Title Page

Using physics-based pose predictions and Free Energy Perturbation calculations to predict binding poses and relative binding affinities for FXR ligands in the D3R Grand Challenge 2

Authors

Christina Athanasiou,[1] Sofia Vasilakaki,[1] Dimitris Dellis,[2] Zoe Cournia[1,*]

Affiliations

1. Biomedical Research Foundation, Academy of Athens, 4 Soranou Ephessiou, 115 27 Athens, Greece

2. Greek Research and Technology Network, S.A., 7 Kifissias Ave, 115 23 Athens, Greece

***Corresponding Author**

e-mail: zcournia@bioacademy.gr

Tel: +30 210 6597195

ORCID

Christina Athanasiou 0000-0003-2973-3550

Sofia Vasilakaki 0000-0002-1008-7264

Zoe Cournia 0000-0001-9287-364X

Keywords (4-6 words) Free energy perturbation · Docking · Farnesoid X receptor · FXR · D3R · FEP+ · Drug Design Data Resource

Abstract

Computer-aided drug design has become an integral part of drug discovery and development in the pharmaceutical and biotechnology industry, and is nowadays extensively used in the lead identification and lead optimization phases. The Drug Design Data Resource (D3R) organizes challenges against blinded experimental data to prospectively test computational methodologies as an opportunity for improved methods and algorithms to emerge. We participated in Grand Challenge 2 to predict the crystallographic poses of 36 Farnesoid X Receptor (FXR)-bound ligands and the relative binding affinities for two designated subsets of 18 and 15 FXR-bound ligands. Here, we present our methodology for pose and affinity predictions and its evaluation after the release of the experimental data. For predicting the crystallographic poses, we used docking and physics-based pose prediction methods guided by the binding poses of native ligands. For FXR ligands with known chemotypes in the PDB, we accurately predicted their binding modes, while for those with unknown chemotypes the predictions were more challenging. Our group ranked #1st (based on the median RMSD) out of 46 groups, which submitted complete entries for the binding pose prediction challenge. For the relative binding affinity prediction challenge, we performed Free Energy Perturbation (FEP) calculations coupled with Molecular Dynamics (MD) simulations. FEP/MD calculations displayed a high success rate in identifying compounds with better or worse binding affinity than the reference (parent) compound. Our studies suggest that when ligands with chemical precedent are available in the literature, binding pose predictions using docking and physics-based methods are reliable; however, predictions are challenging for ligands with completely unknown chemotypes. We also show that FEP/MD calculations hold predictive value and can nowadays be used in a high throughput mode in a lead optimization project provided that crystal structures of sufficiently high quality are available.

1. Introduction

Rational drug design using computational techniques is becoming an essential tool in assisting fast and cost-efficient lead discovery and optimization, due to the fact that it utilizes the information of the three-dimensional structure of the biological target in the process (structure-based drug design) and/or the activity of known binders to the target of interest (ligand-based drug design). The Drug Design Data Resource (D3R) is a community, which collects protein-ligand datasets and organizes international blinded prediction challenges using these resources. As in D3R Grand challenge 2015, this year's D3R challenge provided blinded datasets, which contain binding affinities of multiple ligands against a target protein and co-crystal structures. The aim of these challenges is to provide a solid ground for developers and end-users to identify limitations of the contemporary computational methods and opportunities for improvements.

In the lead identification phase, initially one maps the key interactions between ligands and the protein binding site, predicts their binding poses in the protein, and evaluates the energetics of the resulting complexes. The most commonly used methodology is docking and scoring for virtual screening. It is commonly accepted that while docking usually outputs a good estimate of the binding pose, scoring functions usually fail to correctly rank different compounds with an increasing difficulty in congeneric series [1, 2]. Hence, identifying the top-ranked pose as the right binding pose, is still a challenge [3]. This is also reflected to the results of the predictions during D3R Grand Challenge 2015 [4-6]. On the contrary, cross-docking or ensemble docking, i.e. docking of ligands into multiple receptors or conformations of the same receptor, has been proven valuable in the past, by giving more accurate predictions than docking in a single protein conformation [7-9].

The lead optimization phase is currently one of the most costly phases in pharmaceutical development. According to Paul et al [10], lead optimization accounts for a total of $414 million per approved drug. The process of delivering optimized leads of higher affinity than the parent compound and providing coherent structure-activity relationships that can efficiently guide synthetic efforts can now be both time- and cost-efficient using reliable computational methods to calculate protein−ligand binding affinities. Recent advances in computational methods (e.g., more accurate force fields and sampling algorithms) and the emergence of GPU coding are advancing drug discovery lead optimization efforts from approximate to rigorous methods. A rigorous method for calculating relative protein−ligand binding affinities is the Free Energy Perturbation (FEP) framework, which is currently the most accurate qualitative link between experimental and computational studies, [11] when using sufficiently small mutations and an adequate sampling. Janssen, Bayer, and Pfizer recently published in 2016 several prospective applications of relative binding affinity free energy calculations, which are now becoming accessible to the lead optimization stage of the drug discovery process [12-15].

Accurate methodologies to estimate the structure of a protein-ligand complex and the binding free energy of a small molecule to a receptor could lead to the fast and efficient development of novel, potent protein modulators. Current methodologies have many limitations and usually their applicability is limited. The blind evaluation of these methods, by using datasets of structure-related activity of co-crystalized ligands is of a great importance. Such evaluations promote the application of these methods without the use of any bias in their setup such that the results are a true indicator of their limitations and possible pitfalls. This process can further indicate new areas of investigation for the improvement of these methods.

Here, we present the results of the evaluation of binding pose and relative binding affinities predictions using a dataset of co-crystallized Farnesoid X Receptor (FXR) agonists provided by the D3R for the Grand Challenge 2 competition. D3R provided participants with the structures of 102 compounds and requested the prediction of the crystallographic poses for 36 of them. In addition, the prediction of affinities or affinity rankings, for all the 102 ligands, and for the relative binding affinities for two subsets of 18 and 15 compounds were also requested. The dataset of FXR agonists consisted of previously-characterized isoxazole and benzimidazole analogs, two new novel classes of FXR agonists, including sulfonamide and spirocyclic derivatives, and six miscellaneous compounds. We participated in the binding pose and relative binding affinities predictions, but not in the affinities ranking prediction as scoring still suffers from major limitations proven by the low correlation between docking scores and experimental affinities [3].

For the binding pose predictions, we used a combination of docking, and physics-based methodologies such as FEP calculations, metadynamics, and prediction of water occupancy, taking into account all 28 available FXR crystal structures [16-28]. These methods demonstrated excellent results in predicting the crystallographic pose of ligands with known chemotypes in the literature (e.g. benzimidazoles), which have solved crystal structures, and it showed some success in predicting the binding modes of those ligands in the dataset with new scaffolds (e.g., sulfonamides).

For the free energy predictions, we employed alchemical free energy methods. Calculating the absolute binding free energy of a ligand binding to a receptor would be a direct way to evaluate the biological activity of inhibitors/agonists and reduce the time and resources cost required for the development of a drug, by synthesizing only the potent ones. Unfortunately, such calculations are computationally intractable due to the fact that thermal quantities such as entropy cannot be measured directly in a simulation. As a workaround, alchemical free energy methods have been developed and progressed rapidly over the last two decades [29-37]. Here, we present our methodology used for predicting relative binding affinities of ligands bound to proteins. Based on our results, applying FEP calculations has a high success rate in predicting molecules likely to bind with higher affinity than the parent compound as well as compounds binding more weakly than the parent compound, thus saving valuable resources in a lead optimization project.

2. Methods

2.1 Test datasets and timeline of the challenge

The blinded unpublished dataset, courtesy of Roche Pharmaceuticals and curated by D3R, contained 36 high quality crystal structures of the FXR target and binding data (IC_{50}s) for 102 compounds. The challenge consisted of two stages. In Stage 1, participants were provided a dataset with the FXR apo-protein, SMILES strings and SD files of the 36 ligands for pose prediction, and 66 ligands for affinity prediction or ranking. SMILES strings and SD files of two subsets (18 sulfonamides and 15 spirocyclic compounds) were also provided for the calculation of relative binding affinities. In Stage 1, participants were asked to predict the crystallographic poses of the 36 ligands, affinities or affinity rankings for all 102 ligands, and the relative binding affinities for the two designated free energy subsets. The participants could perform any combination of these tasks. Stage 1 opened on 18th September and closed on 22nd November 2016, followed by the released of the crystallographic poses of the 36 ligands and the beginning of Stage 2. In Stage 2, participants were provided with the actual crystal structures and were asked to predict the affinities, or affinity rankings, of all 102 ligands and/or the relative binding affinities for the two free energy subsets. Stage 2 closed on 8th February 2017 followed by the release of FXR agonist IC_{50}s.

We participated in the challenge for the prediction of crystallographic poses for the 36 ligands and for the relative binding affinities for the two subsets. For all calculations we used the Schrödinger Suite 2016-2 [38].

2.2 Ligand clustering and preparation

Initially, we clustered the 36 compounds based on their chemotype (Table 1 and S1). For this purpose, the Canvas tool v2.8 of the Schrödinger Suite [39] was used for the calculation of Tanimoto similarity between the compounds based on their hashed linear 2D fingerprints. The complete cluster linkage method was used. The results of the Tanimoto similarity calculation are presented in Table S2. The 36 compounds with unknown crystal structures have different chemotypes belonging to five different groups: isoxazoles, benzimidazoles, spiros, sulfonamides and six miscellaneous compounds. Compound FXR_1 has a sulfonamide moiety but due to its substantial chemical similarity divergence from the other sulfonamide compounds it was incorporated in the miscellaneous group.

Table 1. Clustering of the 36 compounds provided by D3R based on their chemotype.

Isoxazoles	Benzimidazoles	Sulfonamides	Spiros	Miscellaneous
FXR_4 FXR_23 FXR_33	FXR_6 FXR_7 FXR_8 FXR_9 FXR_13 FXR_14 FXR_19 FXR_20 FXR_21 FXR_22 FXR_24 FXR_25 FXR_26 FXR_27 FXR_28 FXR_29 FXR_30 FXR_31 FXR_32 FXR_35 FXR_36	FXR_15 FXR_16 FXR_17	FXR_10 FXR_11 FXR_12	FXR_1 FXR_2 FXR_3 FXR_5 FXR_18 FXR_34

The LigPrep [40] tool of Maestro 10.6 was used for the preparation of the ligand structures (SI).

2.3 Protein dataset and preparation

The selection of the receptor crystal structure for the binding pose predictions has a significant effect on the successful prediction of an unknown protein-ligand complex [3]. As 28 FXR protein structures are available in the protein databank (PDB) [16-28], the first challenge was to appropriately select a single or multiple protein structures for the pose prediction part of the challenge. A clustering of the structures based on the chemical type of the co-crystallized, native ligands was performed (Table 2) in order to identify any common cores with the compounds provided by D3R. Based on this clustering, we then chose a suitable group of protein structures for the docking calculations for each chemical group of FXR ligands. It was not possible to dock all ligands in one crystal structure because the binding pocket is very wide (Figure S1).

Table 2. Clustering of the available FXR crystal structures based on ligand chemotype [16-28].

Benzimidazoles	Isoxazoles	Steroids	Indoles	Others
3OLF, 3OMK, 3OMM, 3OOF, 3OOK, 3OKH, 3OKI	3RUT, 3P89, 3RUU, 3P88, 3RVF, 3HC6, 3HC5, 3GD2, 3DCT, 3FXV, 3DCU	4QE6, 3BEJ, 1OSV, 1OT7	3L1B, 3FLI, 4WVD	4QE8, 4OIV, 1OSH

The Protein Preparation Wizard tool [41, 42] was used to prepare the protein crystal structures (SI).

2.4 Selection of the co-crystallized water molecules to be retained in the calculations

Water molecules in the binding cavity should be taken into account during the binding pose predictions. Water molecules that consistently appeared in more than three crystal structures were kept. Specifically, in the isoxazole-FXR complex with PDB ID: 3P89, seven water molecules were kept, while for the crystal structures with benzimidazole ligands two water molecules were retained (Figure S2).

In addition, we performed a WaterMap [43-45] calculation in the unligated structure of FXR provided by the D3R organizers (apo structure). WaterMap uses Desmond to run a molecular dynamics (MD) simulation of water molecules in the ligand binding site of a receptor, which is restrained during the simulation. The excess enthalpy and entropy, and thus the free energy of the water sites are then estimated. These quantities can be used as a guide to which water molecules could be advantageously displaced on ligand binding. For the calculations, the apo structure was imported in the WaterMap panel and the binding site was defined by residues Phe288, Leu291, Met294, His298, Ser336, Ile339, Ile356, and Tyr373.

2.5 Docking calculations

The Standard Precision (SP) [46-48] and Extra Precision (XP) Glide [49] v.7.1 were used for the docking calculations. Initially, a grid, which describes the physicochemical properties of the binding sites, was generated by Glide. The van der Waals radii of non-polar atoms were scaled by a factor of 0.8 in order to avoid rejection of sensible poses due to receptor rigidity. Fully flexible ligand docking was performed with the OPLS3 force field. During the calculations, the hydroxyl groups of serine, threonine, tyrosine, and the thiol group of cysteine residues in the binding site were allowed to rotate to capture all possibilities for hydrogen bonding with the ligands.

2.6 Pose prediction protocol

For the pose prediction, we used a combination of computational techniques, depending on ligand chemotype. More specifically, we followed two different methodologies for: a) FXR ligands that share a common core with the available co-crystallized ligands and b) FXR ligands with a novel, completely unknown scaffold.

For FXR ligands with a known scaffold our workflow included: i) choice of protein crystal structure to be used for docking, ii) docking and alignment of the ligand with the most chemically similar co-crystallized ligand based on shape similarity Tanimoto calculations, and iii) minimization of the complexes generated after the alignment. The chemotypes for which we followed this methodology are benzimidazoles and FXR_5, and FXR_34, which have an indole and steroid chemotype, respectively. In cases where two or more binding modes seemed plausible, for example when a double occupancy of an ortho substituent was suspected, we used physics-based calculations such as WaterMap for the binding pocket of the apo structure, binding pose metadynamics, and FEP calculations to decide on the most probable pose. The following will cover a detailed description of these methods.

For FXR ligands with a chemotype that had not been crystallized before, we chose the most appropriate crystal structure based on: (a) shape similarity of the ligand with the native ligands [50, 51], (b) cross docking in all 28 crystal structures, and (c) calculation of interaction fingerprints similarity [52, 53] followed by docking. According to the available FXR crystal structures, in most complexes either Ser336 or His447 or Tyr373 interact with the ligands via a hydrogen bond and Arg331 interacts with the carboxyl group of the ligands, therefore these were the main interactions that were taken into account using the interaction fingreprints similarity. This methodology was applied on the spiros and sulfonamides groups, and FXR_1, FXR_2, FXR_3, and FXR_18 from the miscellaneous group. In case multiple poses were plausible, we performed metadynamics calculations in order to distinguish the most stable among two or more poses.

Whenever unreasonable conformations (based on chemical principles) were obtained, Quantum Mechanical (QM) calculations were employed to obtain the minimum energy structure. A detailed diagram of the pose prediction methodology is presented in Figure S3.

2.6.1 Binding pose prediction for compounds with known chemotypes

Benzimidazoles

Initially, all seven benzimidazole native ligands (Table 1) were docked in the 3OLF crystal structure in order to test whether benzimidazoles have a common binding mode that can be reproduced using 3OLF. 3OLF crystal structure has the highest resolution in the benzimidazole series. However, due to the receptor rigidity during docking calculations, some ligands did not preserve the benzimidazole binding mode as expected, or even if they did, some of them were slightly shifted from 3OLF native ligand position. Because al available native ligands had the same binding mode and their benzimidazole core was almost perfectly aligned, we expected that this would be the case for the dataset compounds as well. Thus, an additional clustering of benzimidazole FXR agonists was performed according to the ring type attached to the amide, which seems to define their specific binding modes in

FXR. Three clusters resulted: those bearing a) an ortho substituted phenyl ring, which were docked in 3OLF, b) a non ortho substituted benzene ring, which were docked in 3OOF, and c) a saturated ring attached to the amide, which were docked in 3OKI (Table S3). Benzimidazole FXR agonists were docked using the protocol described in Section 2.5. Docking was followed by an alignment of the resulting top-scoring benzimidazole pose with the corresponding co-crystallized ligand. For ligand alignment, the "Flexible Ligand Alignment" option in Maestro was used and the common scaffold alignment method was chosen. Subsequently, an energy minimization of the residues around the ligands was performed using the Prime tool of Schrödinger Suite, assuming that the protein will adapt to the ligand binding mode. The "protein_near_ligand" option was used to define the area for minimization. This energy minimization alleviated any clashes between the ligands and the protein residues.

Isoxazoles

To identify the most suitable crystal structure for docking for each of the isoxazole compounds (FXR_4, FXR_23, and FXR_33), the following methodology was pursued. Due to the fact that FXR_4 is structurally considerably different to the native ligands containing an isoxazole ring, a similarity search against all FXR agonists was performed. For this purpose we used the Shape Screening program (SHAPE) [50, 51]. SHAPE performs a conformational search is performed and each conformer is aligned to the query in various ways, and a similarity is computed based on overlapping hard-sphere volumes. The volume scoring was based on Phase QSAR atom types [54] that were assigned and up to 10 conformers were retained per rotatable bond. In the atom-based QSAR models, the atoms of the ligand are represented as spheres of van der Waals radii and atom types are assigned based on whether they are a hydrogen-bond donor, hydrophobic or nonpolar atom. All other options were left to default. Moreover, cross-docking between FXR_4 and the 28 known crystal structures was performed using the XGlide tool of Schrödinger Suite. The results were evaluated by visual inspection and by using the Interaction Fingerprints tool [52, 53]. Interaction fingerprints evaluate the presence or absence of particular types of interactions between a set of FXR ligands and the active site residues of FXR. All possible interactions were included during the calculation and a score, the interactions similarity score, to compare interactions between the input ligands and the receptor was generated (see Results section).

Subsequently, we followed the pose prediction methodology described in Section 2.6. For compound FXR_4, because of its dissimilarity with the other two isoxazoles in the series (FXR_23 and FXR_33), more than one possible conformation was generated and binding pose metadynamics was also used for the ranking of the poses.

After following the same procedure for FXR_23, we noticed that the adjacent amide and isoxazole groups are not in the same plane. Because of the conjugation of the system, the atoms involved are expected to adopt a coplanar conformation due to the delocalization of the electron density of the p orbital. A 1D torsional scan was thus applied for the rotation around the amide-isoxazole bond to investigate the coplanarity of the moiety. For the torsional scan, the Relaxed Coordinate Scan tool within Jaguar [55, 56] was used. The resulting pose was docked using constraints on the desirable conformation of the amide and then aligned with the native ligand using the isoxazole unit as the common core for the alignment. The choice of the crystal structure for FXR_33 was based on the high similarity between the native ligand of 3P89 and FXR_33 (visual inspection).

Miscellaneous

In the miscellaneous group, compounds FXR_5 and FXR_34 have chemotypes previously characterized in crystal structures in the PDB. Thus, FXR_5 was aligned to 3FLI native ligand and then energy minimization of the residues around the ligand was performed to alleviate any clashes. Compound FXR_34 was docked in 1OT7 structure using SP docking and Induced Fit Docking (IFD) [57-60], which allows the protein structure to adjust to the ligand, with core constraints in order to be aligned to 1OT7 native ligand with the maximum common substructure. The default IFD protocol was used: initial Glide docking by using a softened potential, side-chain prediction with Prime for each protein-ligand complex, Prime minimization of the ligand and the residues close to it and finally, SP Glide re-docking of the ligand in the induced-fit receptor structure. Two SP and three IFD poses were generated using this protocol and these were submitted to binding pose metadynamics calculations in order to identify the most stable one.

2.6.2 Compounds with possible double occupancy or multiple binding poses

For compounds that could adopt multiple orientations due to substituent rotations, physics-based methods were used to determine the most energetically-favorable orientation.

WaterMap calculations

The ortho methoxy group orientation in compounds FXR_6, FXR_14, FXR_30, FXR_31, and rotation around the ether bond of FXR_20 could result in a double occupancy of these structures. Therefore, these were superimposed to the water network derived from the WaterMap calculation in the apo structure of FXR as described above (Section 2.4). The conformations for which the docked poses could displace a thermodynamically unfavorable water molecule were chosen.

Metadynamics calculations

For compounds that could adopt multiple orientations due to substituent rotations, such as in FXR_22, FXR_32, FXR_4 and FXR_34, metadynamics calculations were performed using the binding pose metadynamics tool of Desmond [61], for a series of generated poses by docking. For FXR_22, rotation around the bond between the benzimidazole ring and 1-methoxymethyl benzene was performed and two poses were generated. The two poses underwent a series of metadynamics simulations in order to rank them and predict the most stable binding mode. Pose stability is determined by calculating the ligand RMSD fluctuations over the course of the simulation, and the persistence of important interactions (such as hydrogen bonds and π-π interactions) between the ligands and the receptor (or any other cofactors or solvent molecules, if present). Forces are imposed on the ligand, which tend to displace it from its initial position. The stronger the forces needed for the displacement, the more stable the pose is. The initial pose of the ligand is the reference for the RMSD calculation and this is the collective variable for the metadynamics simulation. Several simulations are performed for better statistics and an average is calculated. A Composite Score is then calculated that accounts for the interactions persistence between the ligand and the active site and the average energy-weighted expectation of the RMSD in each trajectory. For the calculation setup, the receptor-ligand complexes were introduced to the calculation panel and default values were used. FXR_32, which also bears a 1-methoxymethyl benzene group, was aligned to the pose of FXR_22, which was the most stable according to the metadynamics calculation.

For FXR_34, although the steroid group was expected to bind in the same way as other native steroid ligands [24, 27], the position of the isophthalic acid was not obvious. Therefore, five distinct poses of this moiety were generated using Glide SP docking and IFD (as mentioned in Section 2.6.1 – miscellaneous compounds), by keeping the steroid part of FXR_34 constrained and aligned to the 1OT7 native ligand. Five structurally distinct poses (1st and 3rd ranked poses from Glide SP and 1st, 3rd and 4th poses from IFD) were submitted to binding pose metadynamics calculations for the assessment of the most stable pose.

For FXR_4, docking generated two equally-probable conformations in the binding pocket and thus binding pose metadynamics calculations were also used to rank them.

Free energy perturbation calculations

For benzimidazole derivatives for which the benzyl group had two equivalent ortho chlorine positions, FEP calculations were used for investigating their probability to occur. FXR_27 was selected as a representative of this group and was subjected to FEP calculations. FXR_24, FXR_25 and FXR_28, which also have ortho substituted benzene rings, were aligned to the pose of FXR_27 resulting from FEP calculations.

In addition, the ortho chloro substitution in FXR_23 can also adopt two equivalent positions and therefore FEP calculations were performed.

2.6.3 Binding pose prediction for compounds with unknown chemotypes

Spirocyclic (Spiros)

Spirocyclic FXR agonists FXR_10-12 have not been previously described in the literature and thus no available native ligands of this chemotype existed in the PDB. To predict this completely unknown binding mode, we first calculated their shape similarity with native ligands from each chemotype in order to choose a suitable protein crystal structure for docking. For this purpose, the SHAPE tool [50] was used to screen FXR_10, FXR_11, and FXR_12 molecules against all known co-crystallized ligands. Each structure was aligned to the query and conformers of the compounds were generated. Similarity was computed based on overlapping hard-sphere volumes. The volume scoring was based on the atom types and Phase QSAR types were assigned (described in Section 2.6.1 isoxazoles group), and up to 10 conformers were retained per rotatable bond. All other options were left to default. FXR_10 was docked in the 3OMM structure proposed by the shape similarity results. SP Glide docking of FXR_10 in 3OMM indicated two equally probable binding modes, with the bromo phenyl ring pointing to two different directions. These poses were subjected to binding pose metadynamics calculations for the assessment of the most stable as described in Section 2.6.2. Compounds FXR_11 and FXR_12 were aligned to the most stable pose of FXR_10.

Additionally, we performed cross docking of FXR_12 in all 28 available crystal structures using the XGlide tool. The protein structures were imported to XGlide in the form of a grid generated by Glide and FXR_12 was docked in all using SP Glide. The choice of the most appropriate crystal structure for docking was then based on the best Glide Score. FXR_10 and FXR_11 were aligned to the chosen FXR_12 conformation.

Miscellaneous compounds

In the miscellaneous group, FXR_1, FXR_2, FXR_3 and FXR_18 did not have a common chemotype with the available co-crystallized ligands. To determine any similarity with native ligands, the SHAPE tool [50, 51] was used to calculate the shape structural similarity between them and FXR_1. The protein crystal structure with the native ligand having the greater similarity score was chosen for docking (Table S2). The three top generated poses from docking were submitted to binding pose metadynamics to predict the most probable binding pose. The choice of the protein crystal structure for docking FXR_2 was also based on shape similarity results. Alignment to the native ligand and energy minimization of the residues around the ligand followed. FXR_3 was cross-docked in all 28 crystal structures using the XGlide tool of Schrödinger suite. The docking poses of FXR_3 were examined for their interactions similarity with the respective native ligand poses. The crystal structure, which was chosen for docking FXR_3, was based on its Glide Score as well as the interaction fingerprints Tanimoto similarity [62]. FXR_18 was docked in the crystal structure chosen by the shape similarity results using SHAPE tool of Schrödinger. After docking, FXR_18 was aligned to the native ligand based on their maximum common substructure using the Flexible Ligand Alignment tool. Moreover, a binding pose metadynamics calculation was employed to identify the most stable conformation of the acetamide group.

Sulfonamides

FXR_15, FXR_16, and FXR_17 possess a pyrrolo or pyrazolo pyridine substituted with a sulfonyl and an amide group, and had no crystallographic precedent in the known FXR literature. In order to assess the maximal similarity of the sulfonamide core with available native ligands, cross docking with the XGlide tool of Schrödinger between the 28 known crystal structures of the protein against these three ligands was used. In order to estimate the stability of the resulting poses, a geometry optimization was performed in Jaguar [55, 56]. We performed QM and not metadynamics calculations because in this case we evaluated the energetics of the resulting conformation and did not assess two or more binding poses. For the calculation, the 6-31G** basis set was used and the DFT level of theory (B3LYP) was applied. The resulting poses were re-docked first with SP Glide and then with XP Glide.

2.7 Relative binding free energy predictions

For the free energy predictions, two compound subsets were provided by D3R. The first subset consisted of 15 sulfonamide analogs and the second subset of 18 spiros analogs (Tables S4 and S5). Each subset includes congeneric series of compounds, allowing the calculation of relative binding free energies by alchemical free energy transformation methods. No experimental data indicating the compounds' binding modes were available.

Relative binding free energies for the two subsets were estimated using FEP calculations. The free energy is associated with the partition function Z by using the following formula from statistical thermodynamics:

$$RT\ln(K_\mathrm{D}) = \Delta G^0_\mathrm{Bind} = -RT\ln\left(\frac{Z_\mathrm{Complex}}{Z_\mathrm{Solvent}}\right), \qquad (1)$$

where K$_\mathrm{D}$ is the dissociation constant and $Z_\mathrm{state} = \sum_i^\mathrm{state} \exp\left(\frac{-E_i}{k_B T}\right)$

This equation would allow calculation of the free energy difference, assuming that we can assess the potential energies of all possible microstates for each state. In practice, this calculation is computationally intractable, and thus we calculate the differences between the binding affinities of two compounds. A relative free energy calculation formula is derived from equation (1) to describe similar systems, avoiding the calculation of the absolute free energies:

$$\Delta\Delta G^0_{\mathrm{A,B}} = \Delta G^0_{\mathrm{B,Bind}} - \Delta G^0_{\mathrm{A,Bind}} = -RT\ln\left(\frac{Z^B_{\mathrm{Complex}} Z^A_{\mathrm{Solvent}}}{Z^A_{\mathrm{Complex}} Z^B_{\mathrm{Solvent}}}\right) = \Delta G^0_{\mathrm{A,BComplex}} - \Delta G^0_{\mathrm{A,BSolvent}}. \qquad (2)$$

By using differences of binding affinities, the calculation depends only on the free energy change of the transformation of system A to system B in the bound and unbound states. The transformation could involve changes in the chemical composition of the systems (Figure 1), and thus resolve the error associated with computing absolute free energies. A more detailed description of the FEP methodology can be found in the SI.

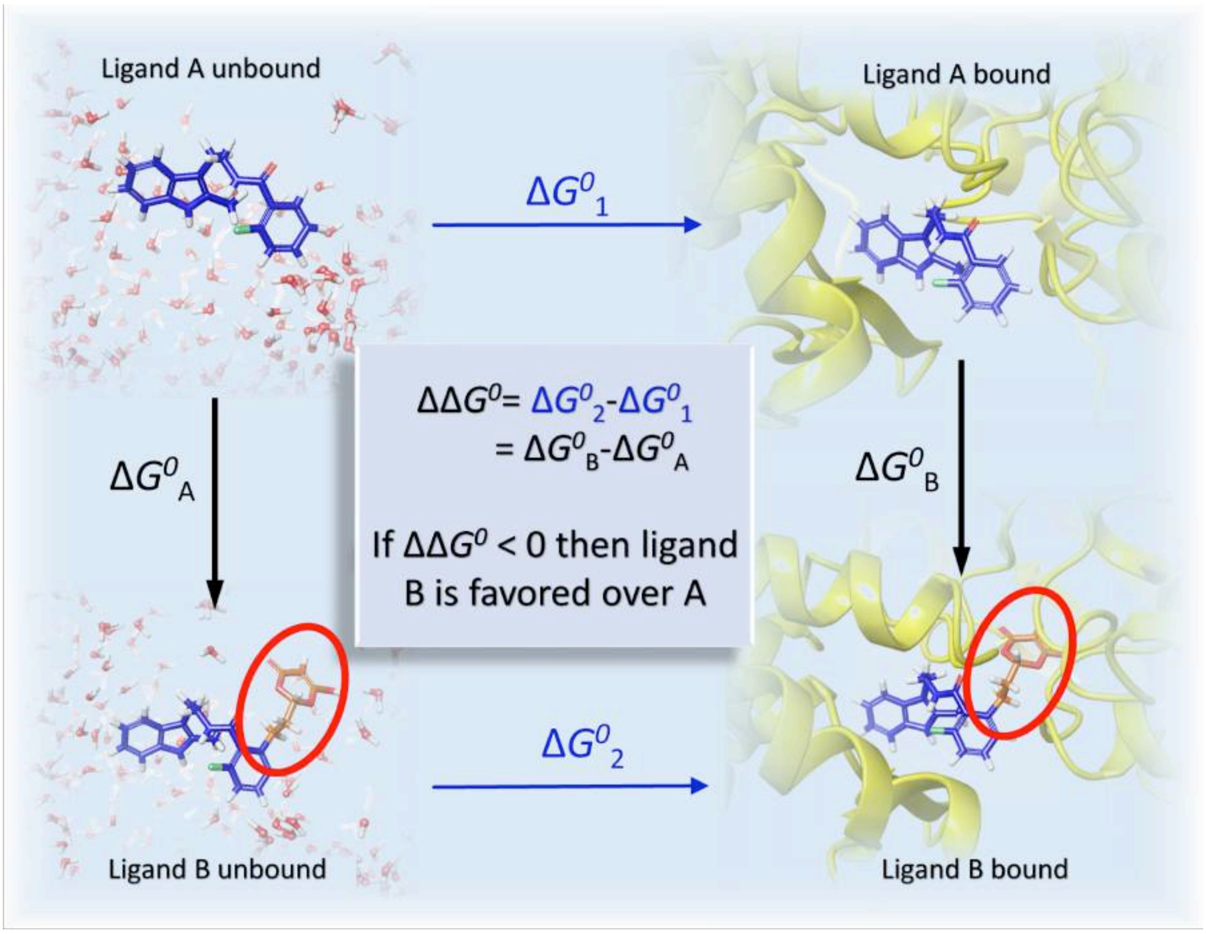
Ligand A unbound
Ligand A bound
ΔG^0_1
ΔG^0_A
$\Delta\Delta G^0 = \Delta G^0_2 - \Delta G^0_1$
$= \Delta G^0_B - \Delta G^0_A$
If $\Delta\Delta G^0 < 0$ then ligand B is favored over A
ΔG^0_B
ΔG^0_2
Ligand B unbound
Ligand B bound

Figure 1. The calculation of the relative binding free energy of ligand B with respect to ligand A, which is the difference ΔG^0_2 - ΔG^0_1, and models the binding process of each ligand to the protein, is computationally intractable. Hence, a closed thermodynamic cycle is contrived. In this cycle, the difference in the free energy between the mutation of ligand A to B in solvent and the same mutation in the complex, i.e. ΔG^0_B - ΔG^0_A, equals to ΔG^0_2 - ΔG^0_1, which is the free energy of interest. The mutation of ligand A to B, which is the addition of the orange substituent (circled in red), is computationally feasible. If this difference in the binding free energy is negative, then it is expected that the binding of ligand B will be more favorable than A.

Obtaining accurate FEP predictions requires overlap of the phase space between the initial (ligand A) and the final (ligand B) state. This is feasible by the introduction of neighboring lambdas (λ), i.e. intermediate alchemical states, along a perturbation path, because larger perturbations generally result in less overlap between the states. When sufficient overlap is not attained, one can either rerun the calculations using more λ windows or insert intermediate compounds. Hence, in order to assure the overlap, an intermediate compound can be introduced to the calculation in order to bridge the conformational space between two ligands for which their potential energies do not sufficiently overlap. For more information about the λ schedule we used here, the reader is referred to the SI.

During a FEP calculation, one ligand from the congeneric series acts as reference to which all other compounds are aligned. In this way, the conserved binding mode as well as the improved overlap between the windows are secured. The reference compound is usually chosen as the compound with the higher certainty of the predicted binding mode, while at the same time it has to be representative of the compound set. In absence of crystallographic data, the choice of the reference compound could be made depending on the highest interactions similarity with the native ligand based on interaction fingerprints. Here, FXR_74 and FXR_17 were chosen as reference structures for the spiros and sulfonamide sets, respectively.

The poses of compounds FXR_17 and FXR_74 were initially generated as described in the pose prediction part of the challenge (see Section 2.6). All structures in the spiros and sulfonamides sets were aligned to their respective reference structures prior to FEP calculations. At the end of Stage 1, the co-crystallized structures of the FXR ligands were released including FXR_10 and FXR_12 from the spiros set and FXR_17 from the sulfonamide set. In Stage 2, we repeated the free energy predictions, considering the real binding poses.

Next, we provide some practical considerations pertaining to the use of the FEP methodology for lead optimization.

2.7.1 The total charge of the system has to be conserved during a FEP calculation

Roux and co-workers have found that changing the total charge during a FEP calculation produced results, which were consistent with experimental data [63]. However, recent studies showed that this approach leads to inconsistent results [2]. More specifically, when a FEP calculation starts from a positively charged molecule and uses a neutral intermediate yields a hysteresis between forward and backward mutations above 2 kcal/mol. Previous studies have shown that turning on or off a charge in a system during a FEP calculation is nontrivial when using Particle Mesh Ewald (PME) for the treatment of electrostatics [64, 65]. The problem arises mainly from the fact that a charge change in PME is handled by introducing a uniform neutralizing background charge to enforce neutrality [66]. In FEP calculations this means that instead of calculating the free energy of turning off/on a charge, the calculated free energy is the sum of turning off/on the charge and the free energy of turning on/off a uniform neutralizing background charge, which might introduce an error in the overall difference in the free energy of binding.

For the D3R challenge, one of the ligands in the sulfonamide subset bears a carboxyl group, which is deprotonated in physiological pH (Table S4). For the spiros subset, the majority (14 out of 18 ligands) also has a carboxyl group (Table S5), while the remaining compounds are neutral. Because ligand charge cannot change during a FEP mutation, all compounds were considered in their neutral form during the calculations.

2.7.2 Alignment to the reference ligand

A primary assumption of FEP is that all ligands in the series retain the same binding mode. Therefore, before conducting FEP calculations, all ligands were aligned to the reference one, with the same procedure followed for pose predictions using the Flexible Ligands Alignment tool of Schrödinger Suite.

2.7.3 Correcting the relative free energy for double occupancy

During Stage 2 of the challenge, the free energy calculations were repeated taking into consideration the real binding mode of the reference ligands into consideration. For the compounds crystallized with a double occupancy, we included both poses in the calculations. In such cases, when the two conformations rapidly inter-convert during the simulation, then the same $\Delta\Delta G$ is expected and the one of the two conformations can be ignored. If one of the two poses is significantly less stable, it can be discounted from the results. Finally, if both compounds maintain separate binding poses, but result to the same binding free energy, the binding free energy for multiple poses can be corrected using equation (3) [67]:

$$\Delta\Delta G_{cor} = -kT \ln\left(\frac{exp(-\beta\Delta\Delta G_{pose1}) + exp(-\beta\Delta\Delta G_{pose2})}{2}\right), \quad (3)$$

where $\Delta\Delta G_{\mathrm{cor}}$ is the corrected binding free energy difference, $\Delta\Delta G_{\mathrm{pose1}}$ and $\Delta\Delta G_{\mathrm{pose2}}$ are the two poses resulting from double occupancy.

2.7.4 Running FEP calculations using the FEP+ tool

All compounds were connected to each other with the use of FEP Mapper panel and the calculation run with FEP+ of Schrödinger Suite. In FEP Mapper compounds are connected with each other with edges, according to LOMAP algorithm criteria [68], i.e. chemical and binding mode similarity, preservation of rings, preservation of ligands charge. The lead optimization mapper (LOMAP) is an automated algorithm for the generation of the most efficient mutations between ligands of a library, according to several criteria such as their chemical and binding mode similarity and the preservation of rings and net charges during the mutations. Additionally, it ensures that each molecule belongs to at least one closed thermodynamic cycle and that the FEP maps, which are created, are spanned by relatively few calculations. Users can define their own connections and cycles, but each compound should be part of at least one closed thermodynamic cycle. In the generated FEP+ map, which shows all the connections between the compounds, each edge represents two perturbations, one in the bound and one in the unbound state (see Results section). The FEP calculations were performed on Tesla K40m GPUs. The running protocol of FEP+ consists of several consecutive steps, which are automatically performed (SI).

2.7.5 Error estimation and convergence

The Bennett Acceptance Ratio (BAR) method was used to estimate the free energy difference of the MD simulations [69]. The errors in the relative free energies were calculated with the cycle closure method using the default scheme applied in FEP+ [11, 70]. After performing a FEP calculation, FEP Mapper identifies unconverged edges, which are FEP calculations between a pair of ligands that have not converged or have not been correctly set up. These edges will contribute to high hysteresis, and FEP Mapper returns them using a color code.

Green indicates a converged edge and unconverged perturbations are colored red. Unconverged perturbations are judged by hysteresis error and also the difference between the raw and predicted ΔG values. For more information see the SI.

To calculate the convergence of each FEP calculation in the FEP Map, the total free energy differences between the two ligands (ΔG in kcal/mol) in solvent and complex legs are plotted as a function of time. In FEP+, three plots for each leg show the accumulated data during different time window schemes: forward; reverse; and sliding window, and the associated bootstrap and analytical error estimates from corresponding simulation legs are also reported. For the sliding window free energy calculations are performed for small windows of the trajectory without averaging from beginning to that point or from the end to that point backwards, similar to a running average. Bootstrapping is a statistic analysis technique, which is used by the program to re-sample the free energy and calculate its variance. The forward time plot presents the cumulative over time free energy from all λ, starting from t=0 ns to t=5 ns for each window, while the reverse time plot presents the cumulative over time free energy from all λ, starting from t=5 ns to t=0 ns for each window (Figures S22-S23). FEP+ performs FEP with Replica Exchange with Solute Tempering (FEP/REST) to enhance the sampling of the ligand. Moreover, the exchange density of FEP replicas over λ windows in the REST simulations is calculated. For more information about FEP/REST enhanced sampling see the SI.

2.7.6 Analysis of FEP calculations

After performing the FEP+ calculations and the convergence check, the differences in the free energy of binding of each compound with respect to the reference ligand are output. For each FEP calculation, visualization of the trajectory was performed to monitor the extent of sampling, (e.g. ring flipping) and also the intermolecular interactions. FEP+ analyzes intermolecular interactions by providing a panel of protein-ligand interactions for λ=0 and λ=1 replicas for each calculation. The specific interactions types assessed and displayed are: hydrogen bond, hydrophobic, ionic and water bridges, which are provided as percentages norrmalized over the course of the trajectory. FEP+ provides a protein analysis report for end-point λ replicas, which contain the RMSD of the protein for λ=0 and λ=1. This report indicates any structural instabilities or conformational changes during the simulation. Also, it calculates the Root Mean Square Fluctuation (RMSF) for each residue to assess any local

changes along the protein chain, overlaid with the experimental B factor.
Finally, a ligand conformational analysis is provided in which rotatable bonds for each ligand are enumerated and color-coded. For each rotatable bond, a representative dihedral angle is monitored throughout the simulation for both complex and solvent legs. The distributions of these conformations are then plotted shown both for the solvent and complex legs. In addition, the potential energy around each rotatable bond is also shown as an overlay of the dihedral angle distribution histograms.

3. Results and Discussion

3.1 Pose prediction for the FXR ligand dataset

Based on native co-crystallized ligand clustering, we chose a suitable group of protein structures for the docking calculations for each chemotype of FXR ligands. The choice of each PDB crystal structure for each ligand is presented in Table S6. At the end of Stage 1, the 36 crystal structures were released for evaluation of the submitted predictions; except for one compound FXR_33, which bore a pyridine group instead of an N-oxide due to oxidation during the growth of the crystal or pyridine as impurity.

3.2.1 Compounds with known chemotypes

Benzimidazoles

Benzimidazole derivatives co-crystalized with FXR were initially docked in the 3OLF crystal structure [25], which failed to reproduce their binding mode. As Figure S5 depicts, although poses of native ligands using 3OLF, 3OMM, 3OOK, and 3OMK structures were correctly predicted, docking could not place properly the phenyl ring bound to the amide linker in the 3OOF native ligand, with a flip of ~90° of the ring taking place.

Comparison of the 3OOF native ligand with the 3OLF ligand shows that the phenyl substituents of the amide are almost vertical to each other. In the 3OOF structure the ring is in the same plane with the amide (satisfying the maximum overlap of the p orbital of the two groups), whereas in 3OLF it is perpendicular to it, probably because of steric clashes between the methyl group and the amide hydrogen. Due to this rotation of the phenyl ring in the 3OLF ligand structure, Met294 approaches the ring to form van der Waals interactions. This is not the case in 3OOF structure, where Met294 points out of the pocket (Figure 2). Consequently, when 3OOF native ligand is docked into 3OLF crystal structure, the steric clashes with Met294 do not allow it to adopt its crystal conformation. Regarding the native ligands of 3OKI and 3OKH crystal structures, which have a saturated ring instead of a phenyl ring, their docking in 3OLF crystal structure performed well for 3OKI ligand (with an RMSD value of 0.5 Å between the predicted pose and the crystal structure), but not for 3OKH ligand (RMSD=1.35 Å).

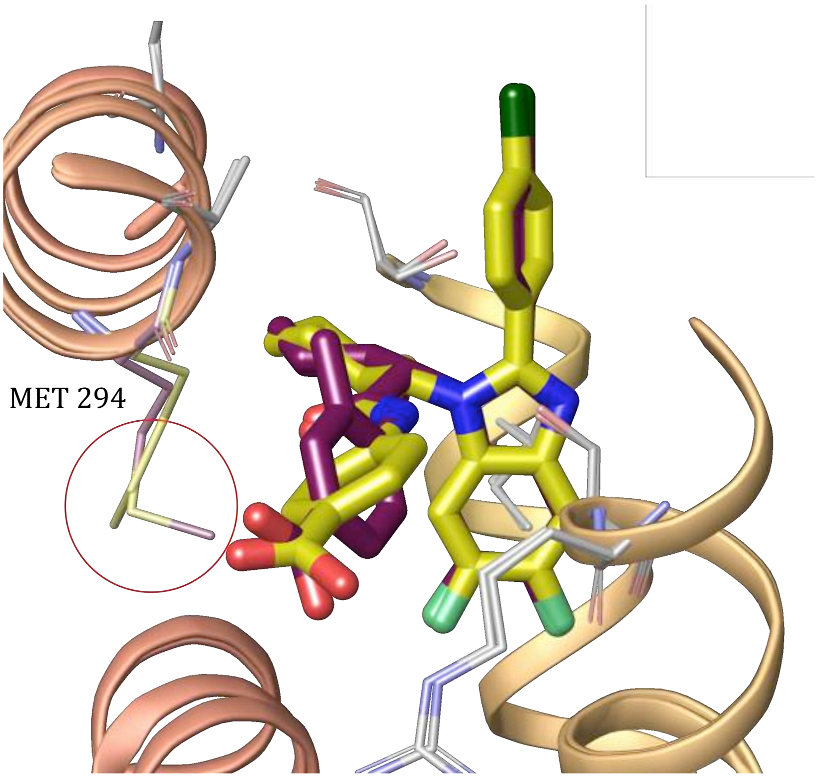

Figure 2. Comparison of the 3OLF (maroon) and 3OOF (yellow) crystal structures. Met294 points towards the ligand in 3OLF structure, while in 3OOF, Met294 points away due to a clash with the carboxyl group.

Therefore, as mentioned in the Methods section, the benzimidazoles were clustered in three groups according to the crystal structure used for the docking. The above procedure secured the conserved binding mode of benzimidazoles. Compounds FXR_7-9, FXR_19, FXR_21, FXR_26, FXR_29, FXR_35-36 binding poses were generated with this methodology, while the remaining benzimidazoles were subjected to further pose optimization. In the majority of these cases (FXR_8-9, FXR_19, FXR_21, FXR_26, FXR_29), predictions were accurate, having an RMSD value lower than 1 Å with respect to the actual crystal structure (Table 3).

Table 3. RMSD (in Å) and ranking results for the 1st ranked poses for all 36 ligands.

Compounds with known chemotypes	**Benzimidazoles**	**3OLF**	
		FXR_14	0.68
		FXR_24	1.19
		FXR_25	0.33
		FXR_27	0.31
		FXR_28	0.86
		3OOF	
		FXR_21	0.8
		FXR_29	0.4
		FXR_36	0.92
		3OKI	
		FXR_6	0.53
		FXR_7	0.52
		FXR_8	0.44
		FXR_9	0.32
		FXR_13	0.56
		FXR_19	0.52
		FXR_20	0.82
		FXR_22	2.2
		FXR_26	0.99
		FXR_30	0.89
		FXR_31	0.54
		FXR_32	2.26
		FXR_35	1.23
	Isoxazoles	**FXR_4**	6.77
		FXR_23	7.76
	Miscellaneous	**FXR_5**	0.38
		FXR_34	3.54
Compounds with unknown chemotypes	**Spiros**	**FXR_10**	2.14
		FXR_11	2.49
		FXR_12	2.48
	Sulfonamides	**FXR_15**	5.66
		FXR_16	1.57
		FXR_17	1.63
	Miscellaneous	**FXR_1**	5.99
		FXR_2	7.47
		FXR_3	8.37
		FXR_18	8.42

For FXR_7, the phenyl thiophene moiety demonstrated a double occupancy (51:49), with our prediction capturing one of the two binding modes (Figure 3) and an RMSD=0.517 Å with respect to the X-ray pose.

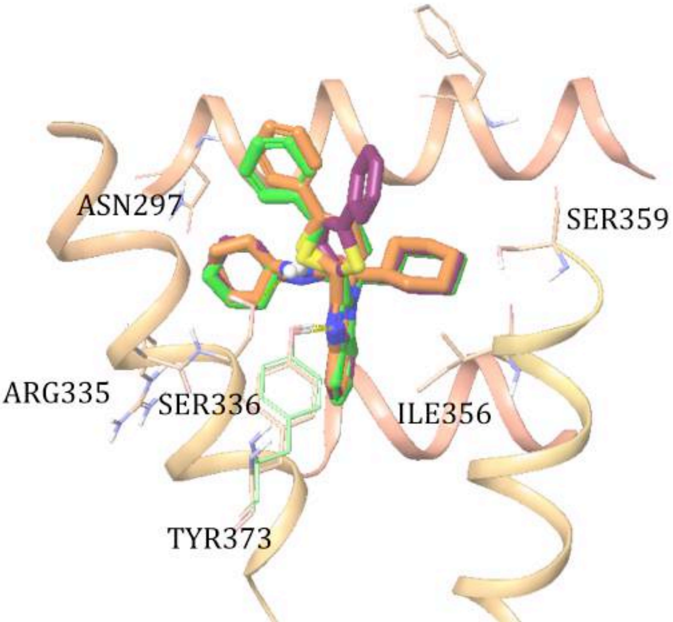

Figure 3. Double occupancy in FXR_7 compound and comparison with our prediction. The two crystal binding poses are presented in orange and purple and the predicted pose in green. The RMSD between the orange and the green poses is 0.52 Å.

Interestingly, for FXR_35, although the predicted binding mode is consistent with the experimental one, the RMSD is higher than 1 Å. This is due to the flip of the cyclohexylmethanesulfonic acid moiety, possibly occurring from the retained water molecules in the structure, where the ligand was docked, and which are displaced in the crystal structure (Figure 4 left). FXR_36 RMSD value, which is close to 1 Å, is a result of the inversion of the thiazol ring, the second possible binding mode of which was not examined (Figure 4 right).

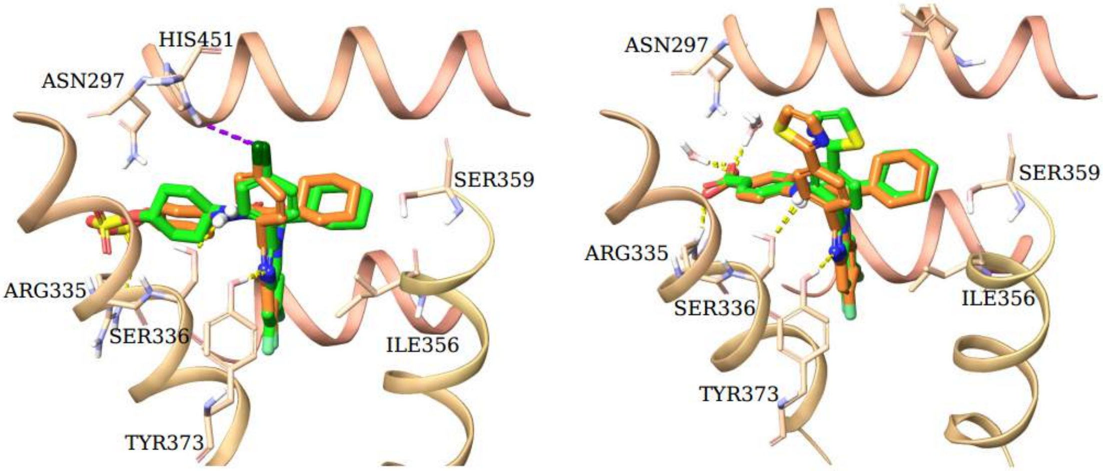

Figure 4. FXR_35 and FXR_36 predicted poses (green) and crystal structures (orange). Left: FXR_35 predicted pose has a flipped saturated ring (RMSD=1.23 Å). Right: FXR_36 has an inversed thiazole ring (RMSD=0.92 Å).

In cases where double occupancy was a possibility, e.g. when an ortho substituent could be found in two equivalent orientations, we performed extra calculations described here. Compounds FXR_6, FXR_14, FXR_30, FXR_31 bear an aromatic ring with two methoxy substituents; one in the ortho and the other in the para position. The ortho substituent can occupy both equivalent positions, and in order to identify which of the two is most probable, we used a WaterMap calculation in the FXR apo structure. In fact, we examined whether the methoxy group could replace any thermodynamically unstable waters in either of the two ortho positions. Subsequently, superposition of the compound with the water network (Figure 5) indicated in which of the two positions methoxy could displace or retain unfavorably or favorably bound waters, respectively. In Figure 5, it is clearly shown that the ortho methoxy on the left position of FXR_6 benzene ring could replace an unstable water. Therefore, compounds with this specific substituent were submitted at this conformation.

Comparison with WaterMap in apo structure

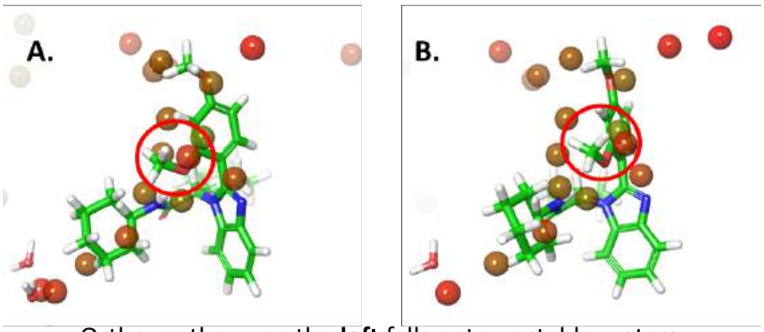

Ortho methoxy on the **left** falls onto unstable waters

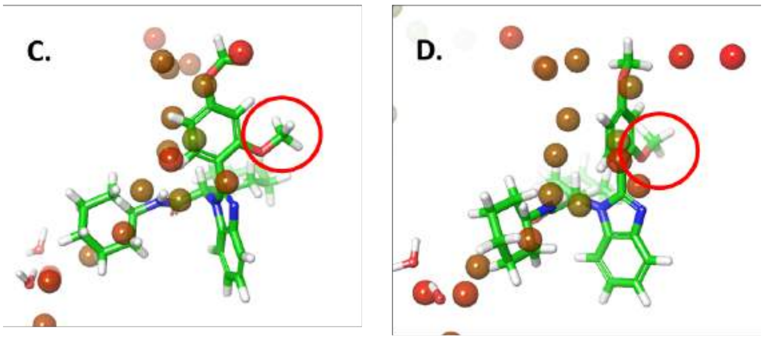

Ortho methoxy on the **right** falls onto the void

Figure 5. Superposition of FXR_6 possible methyl orientations with WaterMap calculation in the apo structure. A and B show the conformation of FXR_6 when the methyl substituent is on the left of the ring and C and D when it is on the right.

Comparison with the actual crystal structures showed that both possible binding modes were correct in the cases of compounds FXR_6 and FXR_14, since their 1,3-dimethoxybenzene ring has double occupancy (Figure S6).

On the contrary, FXR_30 and FXR_31, which bear a 2,6-dimethoxypyridine instead of a dimethoxybenzene ring, do not display two possible interchangeable binding modes. In this case, the predicted poses using the water networks, were correct.

Comparison with the water network retrieved from the WaterMap calculation in the apo structure was also conducted for FXR_20. The methyl group in the chloro benzene ring should point in the same direction as for FXR_6, so as to displace an energetically unfavorable (unhappy) water (Figure 5).

Surprisingly, both poses occurred during crystallization, but this time not in the double occupancy form, i.e. they do not rapidly interconvert. Instead, the crystallized structure consisted of two crystal monomers and in each chain FXR_20 adopts the two different conformations. This means that FXR_20 adopts both poses in the binding pocket, but once it binds to the protein, conserves its pose with no interconvertion. According to the D3R guidelines, only the lowest RMSD between submitted poses was considered, thus this submission resulted in an RMSD of 0.82 Å (Figure S7).

For FXR_22 because of the rotation of the (1-methoxymethyl)benzene group, two poses of FXR_22 were generated by docking and were evaluated for their stability using a binding pose metadynamics simulation. The results indicated the pose of the Figure S8A as the most stable. Based on this, a similar conformation was submitted for FXR_32, which bears a (1-methoxymethyl)benzene group in the same position. However, the CompScore, from the FXR_22 metadynamics calculations was 1.003 for the first ranked pose versus 1.113 for the second one. Their difference is negligible and perhaps this explains why the other conformation was the correct one, with an RMSD value of 0.71 Å versus 2.20 Å of the submitted pose (Figure S8).

To assess the most probable orientation of the ortho substitution in the amide bound benzene ring of FXR_24, FXR_25, FXR_27 and FXR_28 compounds, we used FEP calculations. In detail, the relative binding free energy between the two equivalent positions of chlorine in FXR_27 was calculated and the thermodynamically most favorable was submitted. According to the calculation shown in Figure 6, the FXR_27 pose with the chloro substituent pointing up is energetically more favored than the other. Thus, all four compounds were submitted having a similar conformation.

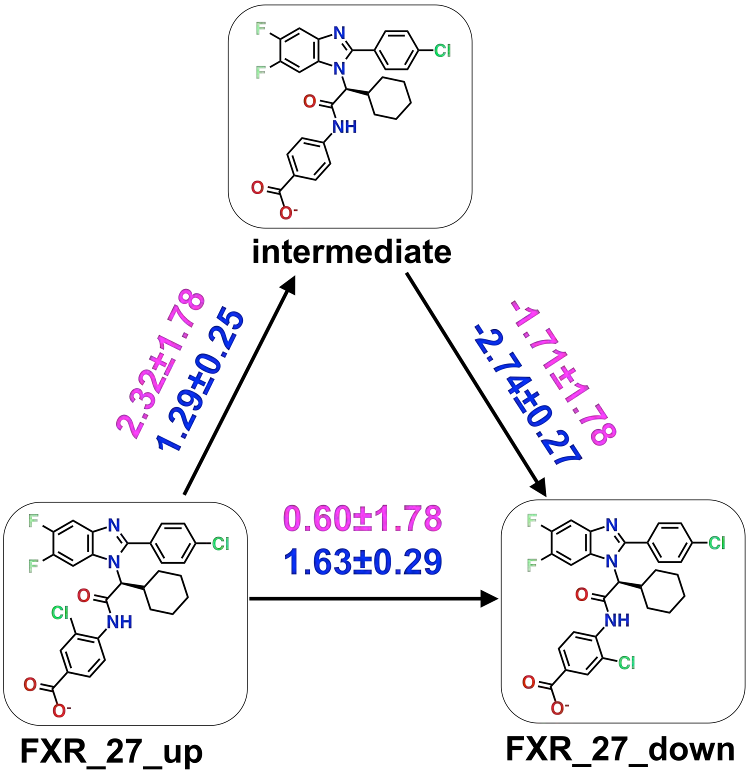

Figure 6. FEP results for the identification of the most stable pose of the ortho substituent for FXR_27. The cycle closure free energy values are indicated in purple and the raw values in blue (in kcal/mol). The large difference between the two values is due to the high hysteresis of the cycle (Δ=-3.08 kcal/mol).

Indeed, this prediction was successful for FXR_27 and FXR_25 (Figure 7 upper panel), but not for FXR_24 and FXR_28 (Figure 7 lower panel), which have an ortho fluoro substitution in the benzene ring, attached to the amide. In FXR_24 the ring flips by 180°, while in FXR_28 it turns approximately 50°. It is possible that this flip in the case of FXR_28 happens because in this conformation the p orbital of the benzene ring and the ether oxygen have the optimal overlap without the fluorine making any steric clashes as in the case of the amide in FXR_24, 25, 27.

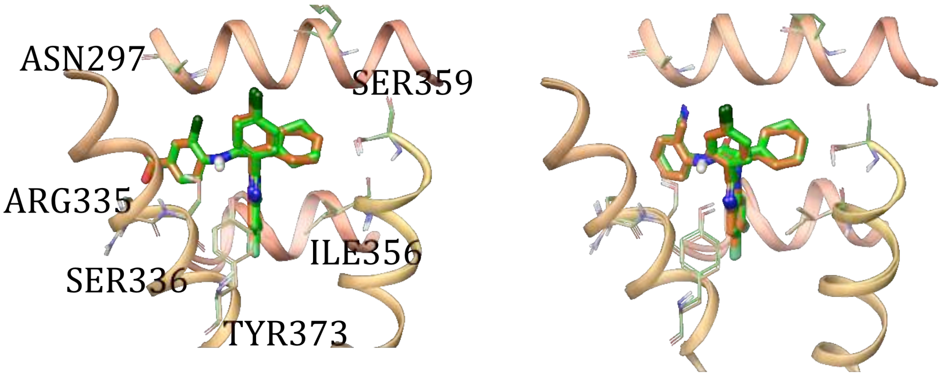

FXR_27 **FXR_25**

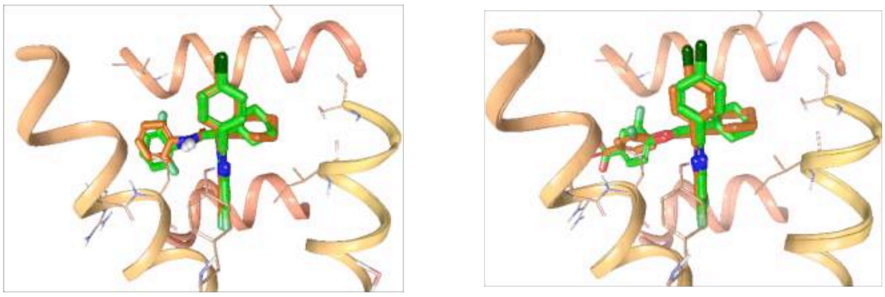

FXR_24 **FXR_28**

Figure 7. Ortho substitutions in benzene ring of FXR_27 (RMSD=0.31 Å), FXR_25 (RMSD=0.33 Å), FXR_24 (RMSD=1.19 Å) and FXR_28 (RMSD=0.86 Å).

Miscellaneous

From the miscellaneous group, compounds FXR_5 and FXR_34 have common chemotypes with native ligands available in the PDB. Specifically, FXR_5 is almost identical with the co-crystallized ligand in 3FLI crystal structure. Their only difference is that 3FLI ligand has an isopropyl formate group attached to the heterocyclic ring instead of an ethyl formate as is the case of FXR_5. Thus, for FXR_5, the same methodology as for benzimidazoles was applied. As expected, FXR_5 maintained the binding mode of 3FLI native ligand (Figure S9).

Compound FXR_34 has a steroid core. There were four crystal structures in PDB with a steroid native ligand and we used 1OT7 as a guide to obtain FXR_34 binding mode. The steroid part of FXR_34 was expected to be found in the same location and orientation with 1OT7 ligand, however, the conformation of the isophthalate ring was ambiguous. Therefore, binding pose metadynamics calculations were used in order to identify the most stable pose. Because these calculations can only distinguish the most probable pose among others, and not generate a predicted one, two poses of FXR_34 ligand were generated by SP docking and three by IFD. In both calculations, core constraints were applied to the steroid ring of FXR_34, so as to be perfectly aligned to that of 1OT7 ligand. The five poses of FXR_34, which were evaluated by metadynamics simulations for their stability are shown in Figure S10.

Unexpectedly, the FXR_34 crystal structure revealed that the steroid moiety adopts a different conformation in the pocket (Figure 8), in contrast to the crystal structures with co-crystallized steroid native ligands (PDB IDs: 4QE6, 3BEJ, 1OSV, 1OT7). Admittedly, FXR_34 ligand bears a major alteration in its chemical structure with respect to the steroid ligands from the PDB. This is a clear example of a ligand modification, which leads to an alternate binding mode and may result in incorrect interpretations in structure-based drug design. None of the participants accurately predicted the correct pose (RMSDs>2 Å).

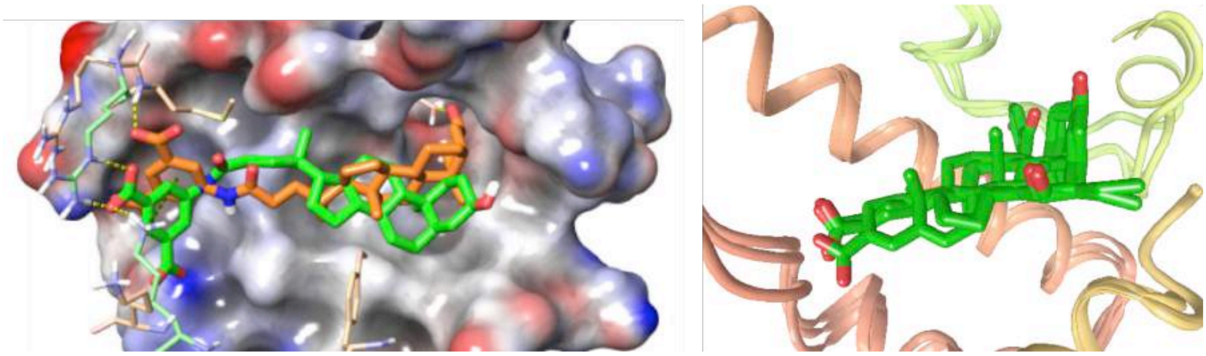

Figure 8. Left: Superposition of the submitted pose of FXR_34 (green) with the crystal structure (orange) (RMSD=3.54 Å). Right: Overlaid steroid ligands crystal structures available in the PDB.

Isoxazoles

FXR_4, FXR_23 and FXR_33 belong to the isoxazoles group. Although the isoxazole ring is present in many co-crystallized ligands, the shape similarity scan for the FXR_4 showed that its structure is more similar to benzimidazoles derivatives (Shape Similarity Score>0.5, Table S7). Cross-docking of FXR_4 in all FXR crystal structures was also performed. The resulting docked poses were evaluated by visual inspection and the Interaction Similarity score. The docked poses of FXR_4 generated in 3OMK (Fingerprints Similarity 0.46) and 3OOF (Fingerprints Similarity 0.58) were promising for a reasonable prediction of the binding mode. Both structures have been co-crystallized with a benzimidazole derivative, which further supported the SHAPE results. The docked pose in 3OMK was aligned with the co-crystallized ligand and subjected to minimization with Prime to remove any steric clashes with the amino acids of the active site. Docking in 3OOF generated two different conformations of FXR_4 in the binding pocket and thus binding pose metadynamics was used to rank them. The best ranking pose, based on the Composite Score, was also aligned with the co-crystallized ligand, using the maximum common core, followed by minimization in Prime to remove steric clashes. A hydrogen bond between the isoxazole ring and Tyr373 was present in both submitted poses, which further supported our pose choice. Despite this, the co-crystallized FXR_4 revealed an unexpected binding mode (Figure S11). The RMSD results provided by D3R showed that the average RMSD value for the submitted poses was between 1.4-2.8 Å for the first three best predictions and above 3.7 Å for the rest of them.

A torsional scan was applied on the amide bond of FXR_23 to calculate the most preferable conformation. As depicted in Figure S12, the energy is minimum when the conformation of the bond is almost planar. 3P89 protein structure was selected to be used for docking FXR_23, based on shape screen against all the available crystal structures (Shape Similarity Score>0.5) and the cross docking results (Fingerprints Similarity 0.64). The docked pose was aligned with the co-crystallized ligand and subjected to minimization in Prime. Taking into consideration the double substitution of the phenyl group of the co-crystallized ligand, we decided to investigate further the position of the chlorine atom of the mono-substituted phenyl group of FXR_23. For this, FEP calculations were used to provide an estimate of the difference between the binding affinities of the two different conformations (Figure S13). The co-crystallized FXR_23 revealed that the isoxazole moiety does not occupy the same area as in the known structures, rendering it difficult to predict an accurate binding pose.

3.2.2 Compounds with unknown chemotypes

Spirocyclic

The spiros group was among those with no native ligands of the same chemotype available and thus their binding mode was completely unknown. In order to choose in which crystal structure they should be docked, we first calculated their shape similarity with some representative native ligands from each chemical type using the SHAPE tool. SHAPE performs a 3D scan of the molecules in order to identify the maximum overlapping volume. Although the results generated by SHAPE indicated that the native ligand of 1OT7 displays the highest shape similarity with all three spiros molecules (see Table S7), they had little chemical similarity. As a result, 3OOM was used instead of 1OT7, which was the second structure according to SHAPE results with high shape similarity and better chemical similarity.

Compounds FXR_10 and FXR_12 belong to the free energy predictions subset. Because FXR_74, also a spirocyclic compound, was used as the reference in the free energy perturbation calculations, we used this compound for the prediction of the binding mode of the spiros group. Therefore, the FXR_74 predicted binding mode was also used for FXR_10, FXR_11 and FXR_12 predictions. SP Glide docking of FXR_74 in 3OMM indicated two possible binding modes, with the bromo phenyl ring pointing to two different directions (Figure 9). In order to identify the most favorable conformation, three poses of FXR_74 from SP docking as well as two additional poses generated from an IFD calculation in 3OMM structure were used as input in the metadynamics simulations. The calculations indicated the upward pose as more stable, to which FXR_10, FXR_11 and FXR_12 compounds were aligned.

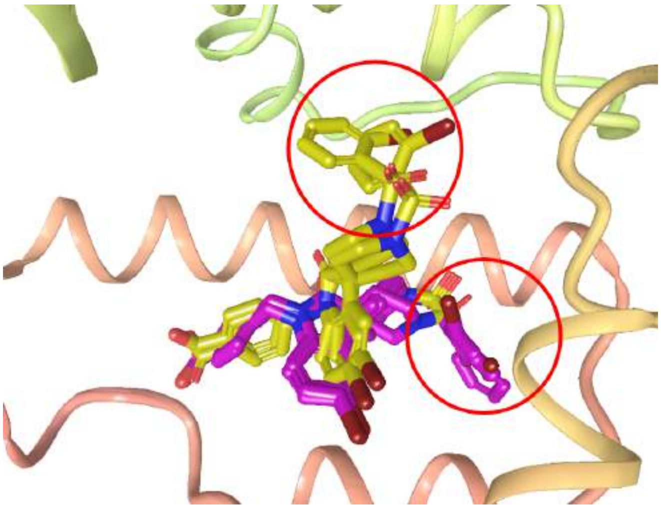

Figure 9. The FXR_74 poses subjected to metadynamics calculations for the determination of the most stable one. The three poses from SP docking are shown in yellow and the two poses from IFD are shown in purple. Inside the red cycles, the two possible binding modes are shown.

Additionally, cross-docking calculations were performed for FXR_12. Comparison of Glide Score values for FXR_12 in each protein structure suggested that the pose generated in 3FXV crystal structure was the most favorable (Glide Score of -11 kcal/mol). Subsequently, compounds FXR_10 and FXR_11 were aligned to the docked 3FXV pose of FXR_12. Both binding modes for each of the three compounds were submitted in Stage 1 of the challenge. The results showed that the pose in 3FXV structure (which was submitted as the first ranked pose), was more accurate than the pose in 3OMM attesting that the cross docking has a higher possibility to generate a pose close to the crystal one. Nevertheless, the RMSD value of this pose was greater than 2 Å (Figure 10).

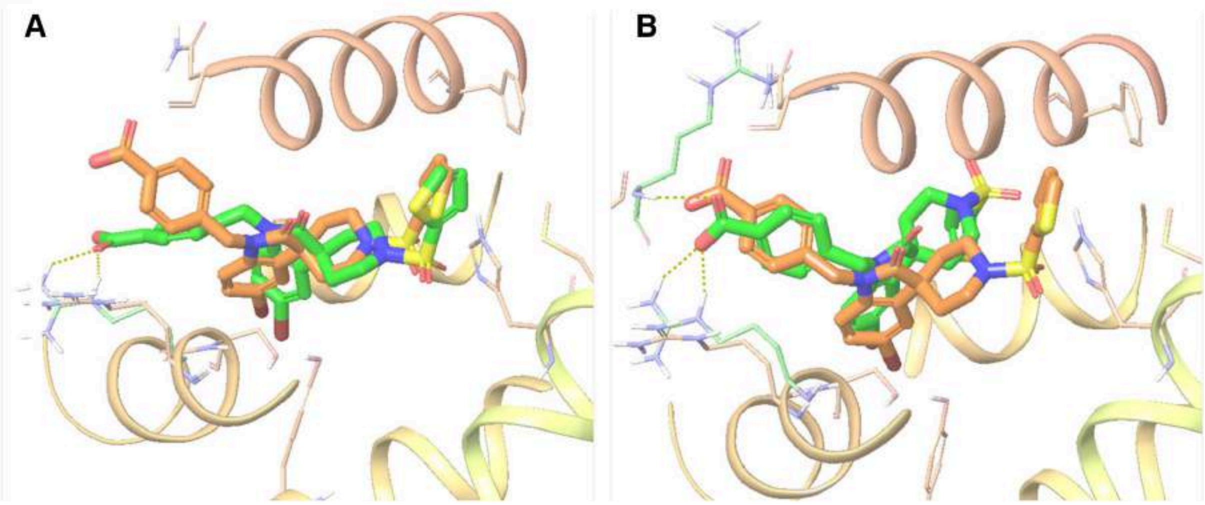

Figure 10. Results for FXR_10 for the two submitted poses. A: RMSD=2.14 Å. B: RMSD=4.43 Å (submitted pose (green) overlaid with the crystal structure (orange)).

Miscellaneous

From the miscellaneous group, compounds FXR_1, FXR_2, FXR_3 and FXR_18 did not have any chemical similarity with the available FXR native ligands.

Initially, SHAPE was used to identify possible shape similarities between the native ligands and FXR_1. However, no structure had high similarity with FXR_1 and therefore cross docking was performed against all 28 proteins, followed by visual inspection. Prediction of FXR_1 binding mode was challenging as docking across the available crystal structures generated diverse binding poses of the compound. The docking pose generated by using

3OKH crystal structure overlapped with the native ligand better than the other cross docking results. The RMSD value of our submitted pose was 5.99 Å and the reported RMSD values of the participants were ≥4 Å, confirming the difficulty in predicting its binding pose. For FXR_2, calculation of its shape similarity with certain native ligands, indicated ligands from 1OSH and 3OKH crystal structures as the most similar. After visual comparison of FXR_2 structure with 1OSH and 3OKH ligands, we found that FXR_2 has a high scaffold similarity with 3OKH benzimidazole ligand, even though they belong to entirely different chemical series. Thus, FXR_2 was docked in 3OKH crystal structure and subsequently aligned to 3OKH native ligand. After the alignment, the protein residues close to FXR_2 were energetically minimized. Unfortunately, this procedure was not successful, since the submitted pose had an RMSD value of 7.47 Å (Figure S14). None of the participants submitted an accurate prediction of this compound pose, indicating its intricate nature.

FXR_3 compound was also cross-docked in all FXR crystal structures and the resulting poses were examined for their interactions similarity with respect to the native ligand. According to Glide Score, 3RUT crystal structure was the most proper for FXR_3 docking with a Glide Score of -11.1 kcal/mol, while the interaction fingerprints Tanimoto similarity indicated the 3FLI structure as the most suitable. The interactions similarity of FXR_3 ligand with 3FLI protein structure with respect to the native ligand's interactions was 0.731 using the Tanimoto metric. Both poses were submitted, but they significantly diverged from the co-crystallized one (Figure S15).

FXR_18 was docked into 3OKH crystal structure, based on shape similarity results using the SHAPE tool of Schrödinger. After docking, FXR_18 was aligned to 3OKH native ligand, followed by energy minimization of the protein residues around the ligands. Next, we defined the position of the acetamide substituent in the benzene ring because it can adopt two equivalent positions (Figure S16 left). Therefore, binding pose metadynamics calculations were carried out to identify the most stable of the two orientations. The results identified the downward pose as the most stable, with a CompScore of -3.378 versus -0.410 for the upward conformation. None of these two pose predictions was accurate, with an RMSD value of 8.42 Å.

Sulfonamides

The cross docking results for the FXR_15, FXR_16 and FXR_17 sulfonamide agonists were evaluated by the interaction fingerprints tools and visual inspection. The 3FLI protein was found to generate better docking results for all three ligands by both the generated conformation of the ligand and the interactions similarity (0.59, 0.53 and 0.61, respectively). In order to estimate the conformations stability, the geometry of the generated poses was optimized in Jaguar. The resulting poses were re-docked first with SP Glide and then with XP Glide. The pose predictions for FXR_16 and FXR_17 are presented in Figure 11.

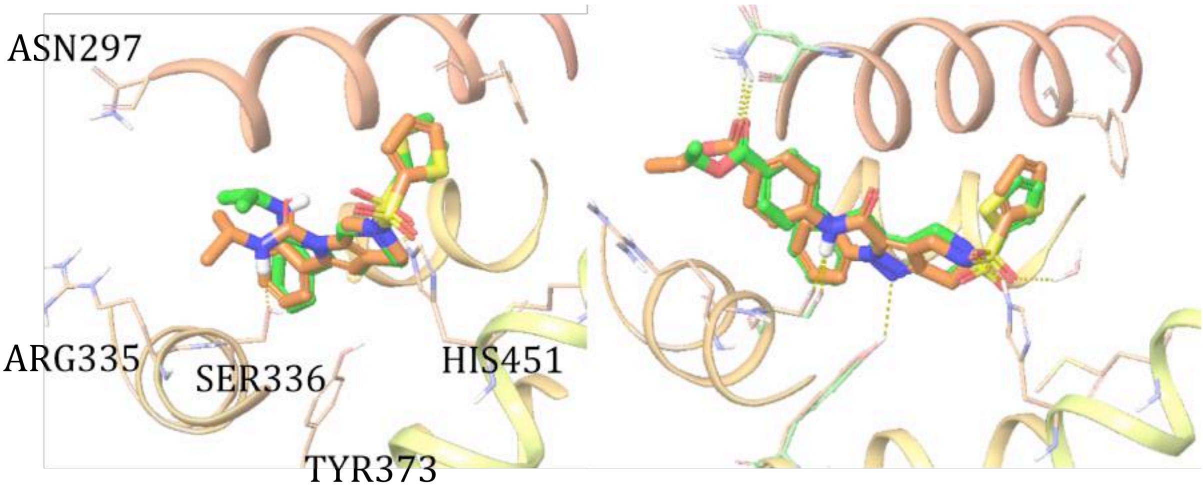

Figure 11: FXR_16 (left) (RMSD=1.57 Å) and FXR_17 (right) (RMSD=1.63 Å) crystal structure (orange) superimposed with the pose prediction (green) in 3FLI.

FXR_15 proved to be a challenging ligand to predict using our methodology (RMSD=5.66 Å, Figure S17), and the RMSD values for the majority of the submitted poses were greater than 4 Å.

All compound predictions together with their respective RMSDs after comparison with the released crystal structure are presented in Figure S18.

According to D3R evaluation results, our predictions ranked #1st out of 49 completed submissions, with a median RMSD value of 0.99 Å. These results validate our methodology, especially for compounds with known chemotype.

3.3 Free energy predictions

The relative binding free energies of the two subsets of ligands were estimated using FEP calculations. The first subset consists of 15 sulfonamides and the second of 18 spiro compounds (Tables S4 and S5). No experimental data existed for the compounds binding modes. Thus, in Stage 1 of the challenge, we performed FEP calculations for the compounds using their predicted binding mode as described above. By the end of Stage 1, among crystal structures released by D3R for the pose predictions part, three structures comprised ligands from the two series (FXR_10, FXR_12 and FXR_17). Participants repeated the free energy predictions for Stage 2, taking into account the real binding poses of these compounds. The prediction of the spiros binding modes has been already described in Sections 2.6.3 and 3.2.2. A primary assumption of FEP is that all ligands in the series retain the same binding mode. Therefore, before conducting FEP calculations, we aligned all ligands to the reference one. In order to identify the reference ligand, we calculated the interactions similarity of all spiros compounds with the native ligand of 3OMM crystal structure. 3OMM was the structure chosen for the docking of the spiros compounds according to shape similarity analysis. The results from the interaction fingerprints Tanimoto similarity are presented in Table S8. Based on that, compound FXR_79 has the higher interactions similarity with the native ligand. However, it is not representative of the spiros group, since it bears a thiophene ring attached to the spiro ring instead of a benzene ring as in the majority of the compounds. At the same time, FXR_84, FXR_85 and FXR_81 (Table S8) were also rejected due to steric clashes with the protein. Eventually, FXR_74 was chosen as the reference compound, which meets both criteria of high interactions similarity and representatively of the spiros group. Consequently, all spiros compounds were aligned to FXR_74 with their maximum common substructure (Figure 12). It should be mentioned here that the interactions similarity with the native 3OMM ligand was calculated only for the spiros compounds, which have a carboxyl group.

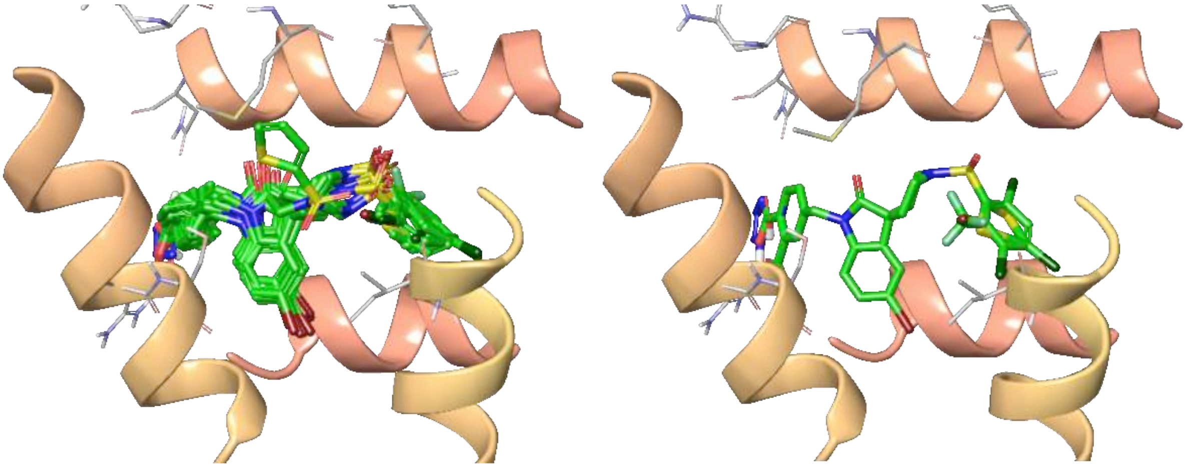

Figure 12. Before (left) and after (right) flexible ligand alignment of the spiros compounds to the reference compound.

To choose a reference ligand for the sulfonamides group, the interaction fingerprints tool was applied in the 3OOF structure (Table S9).

FXR_91 had the highest interactions similarity with the native ligand. Moreover, its structure contains a core present in most sulfonamide compounds but FXR_93. However, FXR_17 has the amide group in a similar position with the native ligand, reproducing the hydrogen bond group with Ser336 and it can be used as a scaffold for reproducing the other molecules of the set. Also, its binding mode was released in Stage 2. As such, it was selected as the representative compound of the set and the rest of the compounds were aligned to it.

The compound sets were then inserted into the FEP Mapper tool of FEP+, which generated the FEP Map of all connections between the two subsets (Figures S19 and S20).

3.3.1 Free energy perturbation results

FEP calculations were run using the predicted binding modes in Stage 1 and were repeated using the real binding modes of spiros and sulfonamides that were disclosed in Stage 2. In Stage 2 compounds FXR_38, FXR_73, FXR_75 and FXR_79, which bear a thiophene ring, were aligned to FXR_10 crystal pose and the rest compounds, which have a benzene ring attached to the spiro core, were aligned to FXR_12. Because FXR_12 demonstrated double occupancy (Figure S21A), with the ortho chloro substitution binding in two equivalent positions, all compounds with substitutions in this ring were considered in both binding modes. As seen in Figure S21B, for compound FXR_85, which has an ortho substituent as well, both poses were inserted in the FEP map. Examination of the trajectories generated by the FEP calculations showed that the compounds retain their separate binding modes without any interconversion, but both poses had about the same binding free energy. For this reason, equation (3) was used to calculate the ΔΔG. FXR_17 did not display any double occupancy, hence the rest of the sulfonamides were simply aligned to it.

The predicted free energies in Stages 1 and 2 as well as the experimental values are presented in Tables 4 (for the spiros) and 5 (for the sulfonamides).

In order to assess the correlation between the experimental and the predicted values, the following formula was used:

$$\Delta G = \mathrm{RT}\ln(\mathrm{IC}_{50}) \qquad (4)$$

where R is the gas constant, T is the temperature and IC_{50} is the half-maximal inhibitory concentration of the ligand provided by D3R. It should be noted that ΔΔG values predicted by free energy perturbation calculations are directly comparable to K_i values, and comparison with IC_{50} values is only possible if the mechanism of inhibition and the substrate concentration are known using the Cheng-Prusoff equations [71], according to which IC_{50} values approximate K_i when the substrate used in the assay is much lower than K_m.

Table 4. Predicted and experimental relative binding free energies ($\Delta\Delta G$) for spiros analogs in kcal/mol.

#Ligand ID	**Predicted $\Delta\Delta G$ (1st stage)**	**$\Delta\Delta G$ Uncertainty**	**Predicted $\Delta\Delta G$ (2nd stage)**	**$\Delta\Delta G$ Uncertainty**	**Experimental $\Delta\Delta G$**	**IC_{50} (μM)**
FXR_10	0	0.4	0	0.4	0	5.64
FXR_12	-1.51	1.73	-3.58	1.1	-2.73	0.058
FXR_38	1.53	0.99	0.5	0.45	1.71	100
FXR_41	-1.84	1.29	-2.08	1.08	1.71	100
FXR_73	1.24	1.6	0.69	0.5	0.41	11.2
FXR_74	-1.93	1.27	-3.69	1.22	-1.28	0.655
FXR_75	1.75	1.31	2.94	0.45	1.71	100
FXR_76	2.41	1.6	-0.41	0.88	1.19	41.8
FXR_77	0.18	1.68	-4.34	1.08	-1.86	0.25
FXR_78	1.74	1.61	-3.66	1.22	-3.16	0.0283
FXR_79	3.62	1.6	0.31	0.5	-0.18	4.15
FXR_81	1.21	1.54	-4.03	1.09	-0.44	2.69
FXR_82	0.35	1.59	-3.05	1.22	-2.05	0.18
FXR_83	-2.59	1.38	-4.61	1.12	-1.69	0.33
FXR_84	-0.07	1.7	-1.65	1.01	-0.13	4.54
FXR_85	-0.02	1.16	-2.79	0.99	-1.75	0.297
FXR_88	-2.23	1.27	-4.39	1	-1.40	0.54
FXR_89	1.15	1.64	-0.14	1.34	-1.21	0.735

Table 5. Predicted and experimental relative binding free energies ($\Delta\Delta G$) for sulfonamide analogs in kcal/mol.

#Ligand ID	**Predicted $\Delta\Delta G$ (1st stage)**	**$\Delta\Delta G$ Uncertainty**	**Predicted $\Delta\Delta G$ (2nd stage)**	**$\Delta\Delta G$ Uncertainty**	**Experimental $\Delta\Delta G$**	**IC_{50} (μM)**
FXR_17	0	0.4	0	0.4	0.00	0.785
FXR_45	-1.05	0.54	0.01	0.43	2.15	28.9
FXR_46	-0.5	0.67	3.41	0.67	2.61	62.4
FXR_47	2.99	1	4.12	1.41	1.96	21
FXR_48	0.72	0.62	1.19	1.05	2.89	100
FXR_49	-0.06	0.61	3.34	0.64	2.89	100
FXR_91	4.35	0.75	5.59	1.1	2.16	29.6
FXR_93	5.55	0.75	5.2	1.41	2.44	46.7
FXR_95	-0.4	0.64	3.17	0.51	2.21	32.2
FXR_96	-0.63	0.54	1.23	0.46	2.57	58.9
FXR_98	-2.17	0.55	2.83	0.6	1.68	13.1
FXR_99	2.35	0.64	4.36	0.58	2.89	100
FXR_100	-0.05	0.64	3.37	1.01	1.90	19.1
FXR_101	5.5	0.8	2.16	1.05	2.12	27.6
FXR_102	5.21	0.75	2.21	1.15	2.16	29.2

The correlation diagrams for Stage 1 and 2 are presented in Figure 14. In the spiros group (Figure 14), this methodology predicted with 85% success (11/13) compounds that have a better binding affinity than the parent compound, as only 2 out of 13 compounds were predicted with the wrong trend. The improvement in R^2 is significant for the spiros group after using the actual crystal structure. For the sulfonamides set though, there is no correlation between the predicted and the experimental values (Figure 14), because of the narrow range of experimental binding free energies, which is within the error of the FEP method (~1 kcal/mol). Encouragingly, all compounds were correctly identified as less active than the reference, which means that in a lead optimization project, these compounds would not have been proposed for synthesis, thus saving valuable resources.

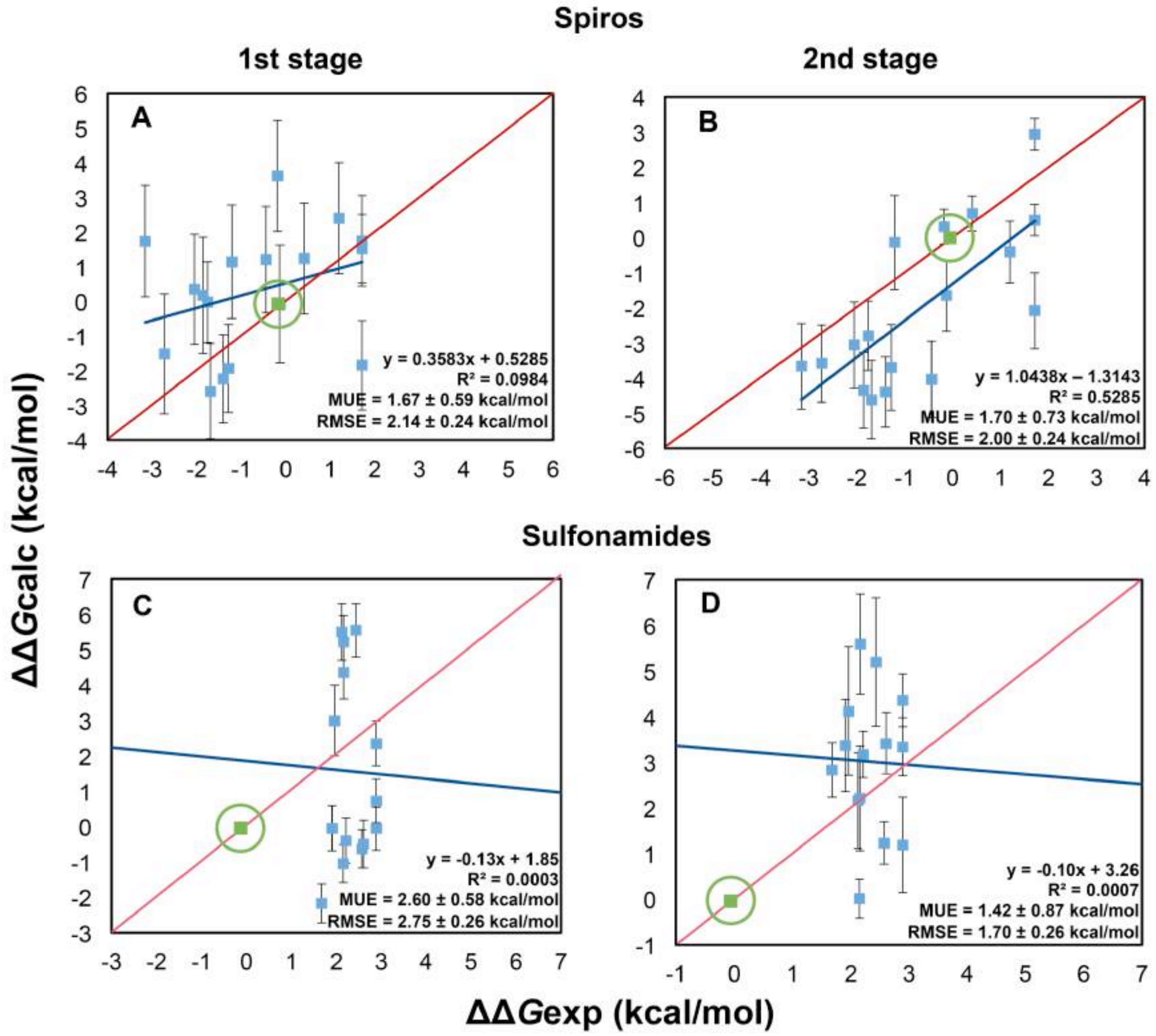

Figure 13. Correlation diagrams of the predicted and the experimental free energies for spiros (A and B) and sulfonamides (C and D) compounds in both stages of the challenge. The y=x line is also shown in red. The point (0, 0), which corresponds to the reference compound, is shown in green square box inside a circle.

3.3.2 Monitoring important interactions

During FEP simulations, crucial interactions were monitored. For example, the two of the most potent compounds, FXR_12 and FXR_78 (IC_{50} = 0.058 μM, and 0.0283 μM, respectively) have an ortho chloro substituent, which can form an additional halogen bond with the residue Leu291 as shown in Figure 15. This extra interaction must be the driving force for the increased potency of FXR_12.

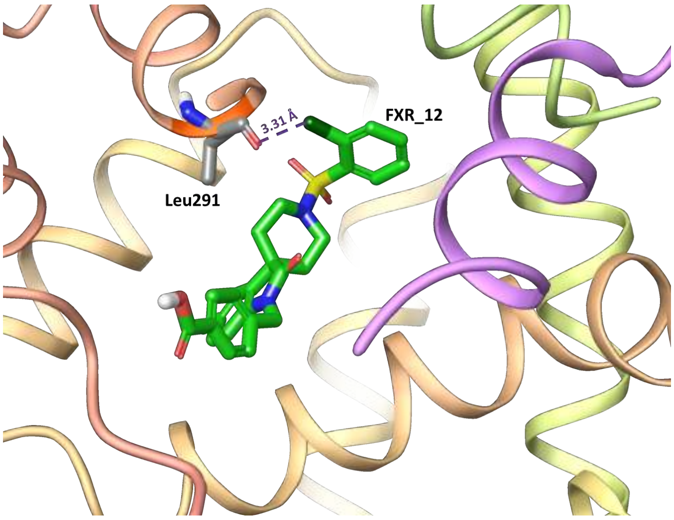

Figure 14. The halogen bond between FXR_12 and Leu291 conserved during the FEP MD simulations.

Also, protein-ligand interactions were investigated using the analysis diagrams produced by FEP+ as seen in an example in Figure 16. Compound FXR_98 has an IC_{50}=13.1 µM compared to IC_{50}=100 µM for FXR_49. Thus, as expected, compound FXR_98 displays more interactions with the protein during the FEP simulation than FXR_49 (Figure 16A). The occupancy ratio of each interaction during the simulation was also reviewed (Figure 16B).

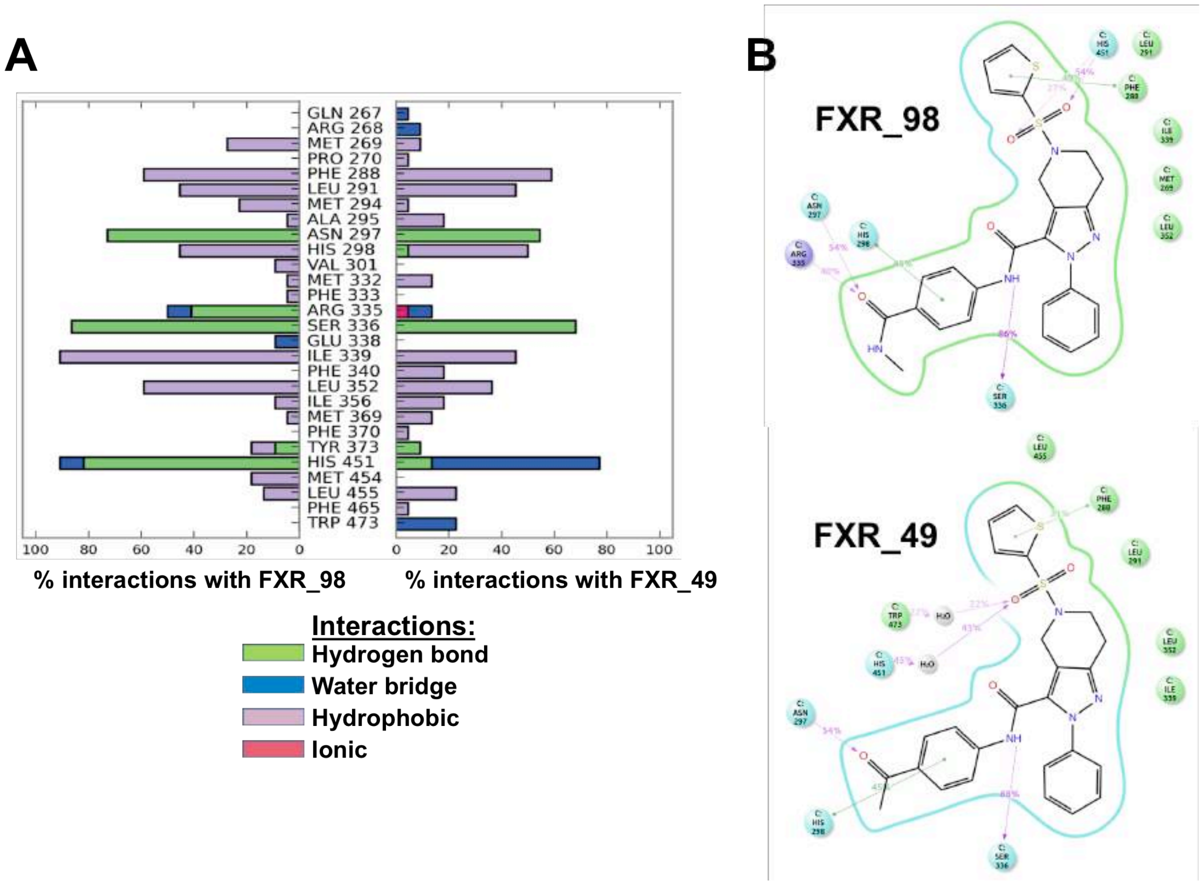

Figure 15. Analysis diagrams produced by the FEP+ simulation. **A.** Comparison graph of the interactions of ligands FXR_98 and FXR_49 with the protein. **B.** 2D interactions diagrams and their occupancy ratio during the simulations.

Moreover, we monitored the distribution of the torsional states of the dihedrals of each compound in the complex and in the solvent (Figure 17). This conformational analysis is useful for indicating any unreasonable conformation of the molecules.

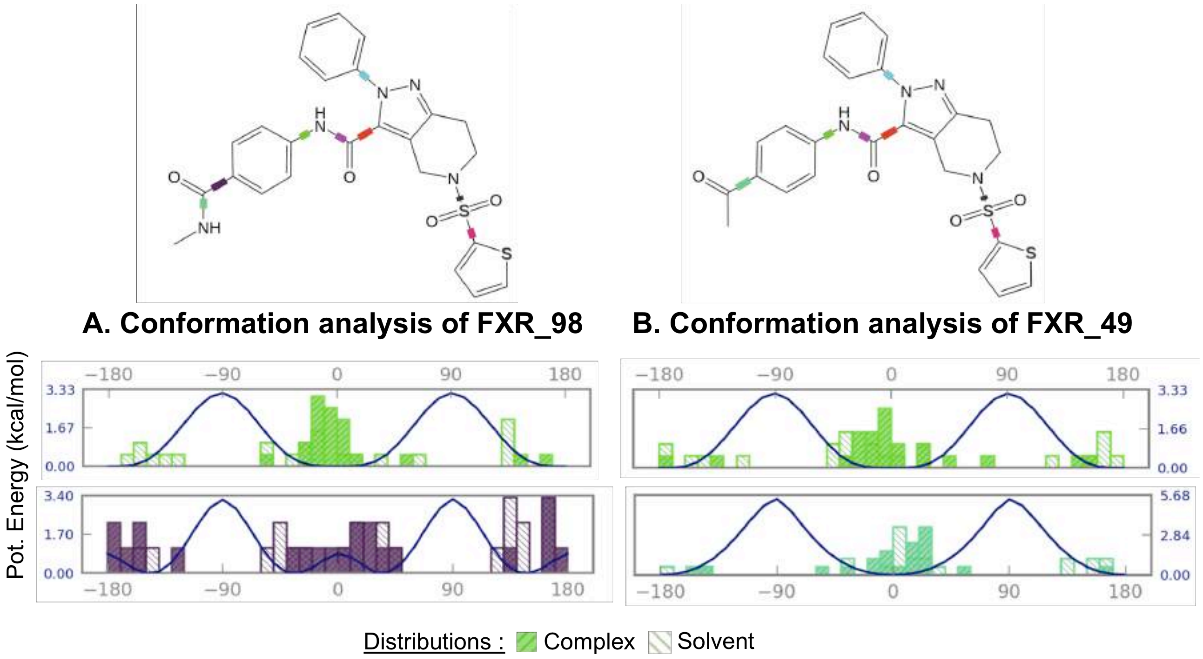

A. Conformation analysis of FXR_98

B. Conformation analysis of FXR_49

Figure 16. Conformational analysis diagrams for FXR_98 and FXR_49. Rotatable bonds in each ligand are represented using a color bar. For each rotatable bond, a representative dihedral angle is monitored during the simulation time for both complex and solvent legs. The distributions of these conformations are then plotted for each bond. Potential energy around each bond overlays the histograms with the blue curve and corresponding labels on the Y-axis.

3.3.3 Convergence of the simulations

Apart from the trajectory analysis, an important consideration is the results convergence. To ensure the free energy convergence, we monitored the cumulative free energy plots over simulation time as explained in the "Error estimation and convergence section (an example is shown in Figure 17, and all convergence plots are provided in the SI, Figure S22-S23).

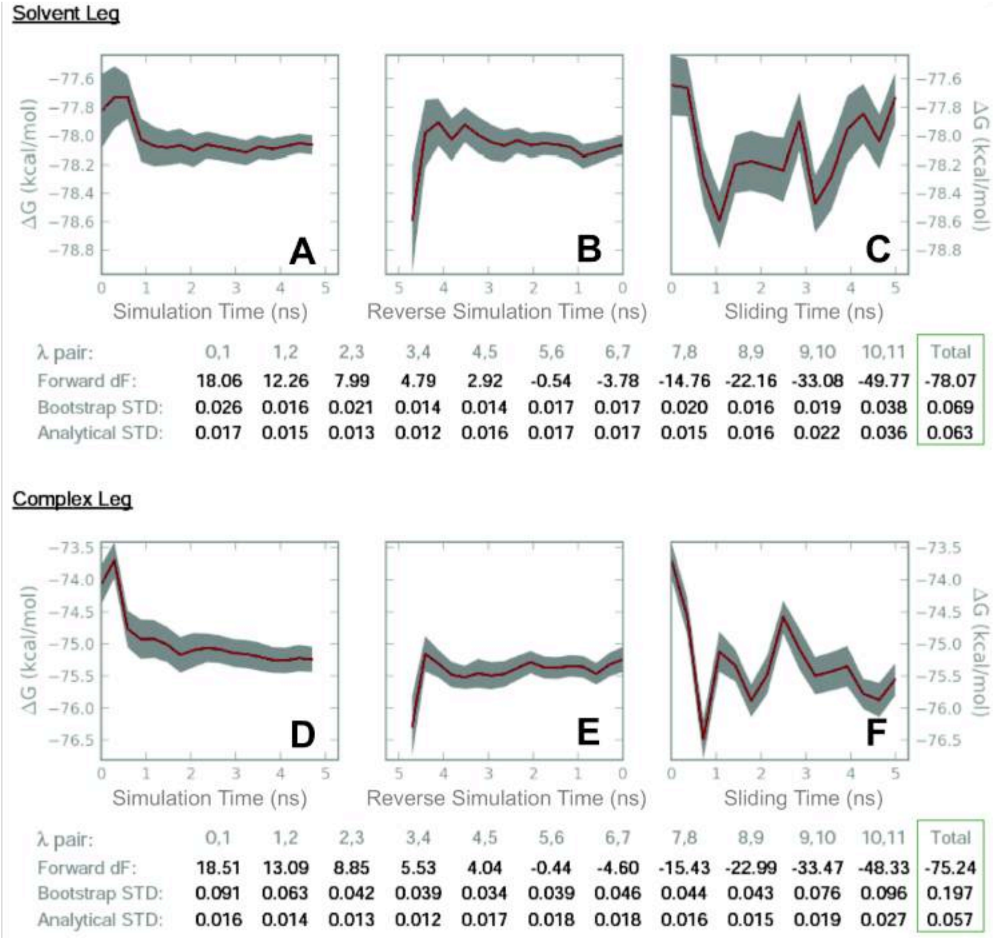

Solvent Leg

λ pair:	0,1	1,2	2,3	3,4	4,5	5,6	6,7	7,8	8,9	9,10	10,11	Total
Forward dF:	18.06	12.26	7.99	4.79	2.92	-0.54	-3.78	-14.76	-22.16	-33.08	-49.77	-78.07
Bootstrap STD:	0.026	0.016	0.021	0.014	0.014	0.017	0.017	0.020	0.016	0.019	0.038	0.069
Analytical STD:	0.017	0.015	0.013	0.012	0.016	0.017	0.017	0.015	0.016	0.022	0.036	0.063

Complex Leg

λ pair:	0,1	1,2	2,3	3,4	4,5	5,6	6,7	7,8	8,9	9,10	10,11	Total
Forward dF:	18.51	13.09	8.85	5.53	4.04	-0.44	-4.60	-15.43	-22.99	-33.47	-48.33	-75.24
Bootstrap STD:	0.091	0.063	0.042	0.039	0.034	0.039	0.046	0.044	0.043	0.076	0.096	0.197
Analytical STD:	0.016	0.014	0.013	0.012	0.017	0.018	0.018	0.016	0.015	0.019	0.027	0.057

Figure 17. The total free energy differences between the ligands FXR_17 and FXR_100 (ΔG in kcal/mol) in solvent and complex legs are plotted as a function of time. Three plots for each leg show the accumulated data during different time window schemes: forward (A and D), reverse (B and E), sliding (C and F) window. The tables report the associated bootstrap and analytical errors estimates from corresponding simulation legs.

4. Conclusions

In the current study, we describe our methodology and results for the prediction of the binding poses of 35 FXR agonists and the binding affinities of two subsets of ligands in the D3R Grand Challenge 2 competition. For the pose predictions, we implemented a variety of techniques after categorizing the dataset ligands into a) ligands with known chemotypes and b) ligands with unknown chemotypes, based on the available crystal structures from the PDB. For ligands with known chemotypes, we initially identified a suitable protein crystal structure for docking, and then docked the ligands to this structure, followed by alignment to the native ligand and minimization. For cases where two or more poses were possible, we performed WaterMap, binding pose metadynamics and FEP calculations to decide the most energetically-favorable pose. For ligands with no crystallographic precedent in the PDB and unknown chemotypes, the choice of crystal structure, to which each ligand should be docked, was very important. For this purpose, we performed shape similarity calculations between the dataset compounds and the native ligands, cross docking in all available crystal structures and interactions similarity calculations. After this step, the ligand was docked to the structure of choice.

The pose predictions for the ligands with known chemotypes were quite accurate with a mean RMSD value of 1.16 Å. Specifically, in the benzimidazole group, alignment to the native benzimidazole ligands, yielded a mean RMSD value of 0.82 Å for all benzimidazoles. This validates our hypothesis that minor ligand modifications do not alter the binding pose. Admittedly, the large number of available benzimidazole ligands in the PDB testifies their conserved binding mode and only major alterations would have been expected to lead to a different pose. Moreover, the majority of the participants predicted benzimidazole binding modes accurately as well. From the miscellaneous group, two compounds possessed known scaffolds and were aligned to the chemically similar native ligands. This methodology was not successful for FXR_34 (steroid core) compound, because the steroid moiety binds in a reverse manner compared to other known steroid FXR agonists. This binding mode was unexpected, since all bile acids, which are believed to be the physiological FXR ligands, bind in the same way. However, binding pose metadynamics successfully distinguished the position of the isophtalate ring, which is more favorable for the binding of the extended side chain.

The two isoxazole compounds, FXR_23 and FXR_33, have a known chemotype. However, the procedure that we followed deviated from the alignment to a native ligand with the same isoxazole scaffold. This decision was based on the chemical diversity of these two compounds from the isoxazole native ligands available in the PDB. Thus, the significant alterations in the structure of these two compounds were assumed to lead to a different binding mode, and therefore a different methodology was used, which resembles the workflow constructed for the ligands with unknown chemotypes. The assumption of the different binding mode proved to be correct, but our predicted poses could not reproduce the crystallographic ones. This result primarily reflects the uncertainty of pose predictions when the pocket is wide and the ligand bears a large structural modification with respect to a crystallized native ligand.

For compounds with unknown chemotypes and specifically for the spiros group, we performed both shape similarity calculations and cross docking, with the second giving better results. Nevertheless, none of these approaches correctly predicted these compounds binding mode, yielding RMSD values higher than 2 Å. This was not the case for sulfonamides, where cross docking results were evaluated by the interaction fingerprints tools and visual inspection, and for which the predictions captured poses close to their co-crystallized structure. Finally, for the miscellaneous compounds with unknown chemotypes, we could not predict their binding mode. This result is partly due to their low molecular weight, which enables them to adopt different configurations in the wide FXR binding pocket. Overall, based on our results, pose prediction is improved when the co-crystalized native ligand has a quantitative shape similarity with the ligand of interest. Assessing the similarity between the native and novel ligands interaction patterns with the protein binding site and preserving those interactions is another factor that leads to improved results.

For free energy predictions, we used the alchemical Free Energy Perturbation framework that predicts relative free energy of binding affinities within a congeneric compound set. Important considerations when using this methodology can be summarized in the following. The starting protein structure has to be of sufficiently high quality and no major conformational changes should be expected during the simulations, as large-scale protein movements cannot be sampled within the timeframe of FEP calculations. Sufficiently long simulations have to be performed and/or enhanced sampling techniques should be applied in order to ensure convergence and overcome conformational ligand barriers. The charge of a ligand cannot change during an alchemical perturbation, and all ligands have to belong to the same congeneric series; perturbations should not be large (normally up to 10 heavy atoms) to allow for configurational overlap between neighboring lambda windows. Examination and choice of buried water molecules to be included in the starting conformation of the calculation is important as these are not expected to exchange with the bulk during the FEP calculation. Before staring a FEP calculation, all ligands need to be aligned to a reference ligand to ensure a conserved binding mode. In case double occupancy is a possibility due to a rotation of a substituent group, both binding modes should be considered in the calculations. The convergence of the simulations needs to be addressed using closed cycles to monitor hysteresis and plotting the free energy differences as a function of time. Care should be taken to compare FEP results with appropriate experimental data. The $\Delta\Delta G$ values predicted by free energy perturbation calculations are directly comparable to K_i values. Comparison with IC_{50} values is only possible if the mechanism of inhibition and the substrate concentration are known; then the relationship between K_i and IC_{50} should be calculated using the Cheng-Prusoff equations [71]. It should be noted that IC_{50} values approximate K_i when the substrate used in the assay is much lower than $K_{m.}$ Finally, the error of the method has been reported to be ~1 kcal/mol, thus a simulation-experimental correlation should not be expected for a narrow range (1-3 kcal/mol) of experimental data.

In this work, binding affinity predictions for the spiros set (Set 2) were successful with 85% success in identifying true positive compounds, i.e. compounds with better binding affinity than the reference (parent) compound. Moreover, the release of the crystal structure in the second stage, significantly improved the correlation between experimental and calculated values, which is consistent with the fact that FEP+ has high predictive ability, given a high quality initial structure. In the sulfonamides subset, no correlation was observed between experimental and predicted data. This is attributed to the narrow range of the experimental values (1 kcal/mol), which is below the method's error (~between 1-2 kcal/mol), which indicates that such an experimental set is not suitable for performing alchemical free energy calculations. It is encouraging, though, that FEP correctly identified all compounds in this subset were true negatives (here defined as compounds that had worse binding affinity than the parent compound) and therefore none of these would have been proposed for synthesis in a lead optimization project.

Concluding, computational methods in drug design have shown significant advances over the years, and future developments are expected to lead to more cost- and time- efficient strategies for the expensive stages in the drug design pipeline such as the lead optimization phase.

Acknowledgements

The research leading to these results has been co-funded by the European Commission under the H2020 Research Infrastructures contract no. 675121 (project VI-SEEM). Computational time was granted from the VI-SEEM project and the Greek National HPC facility - ARIS under the project ID "D3R". Schrödinger representatives are acknowledged for their technical support. All data is available to download at: http://hdl.handle.net/21.15102/VISEEM-277.

This is a post-peer-review, pre-copyedit version of an article published in the Journal of Computer Aided Molecular Design. The final authenticated version is available online at: http://dx.doi.org/ 10.1007/s10822-017-0075-9.

References

1. Baggett, A.W., et al., *Structural characterization and computer-aided optimization of a small-molecule inhibitor of the Arp2/3 complex, a key regulator of the actin cytoskeleton.* ChemMedChem, 2012. **7**(7): p. 1286-94.
2. Gkeka, P., et al., *Free Energy Calculations Reveal the Origin of Binding Preference for Aminoadamantane Blockers of Influenza A/M2TM Pore.* J Chem Theory Comput, 2013. **9**(2): p. 1272-81.
3. Lionta, E., et al., *Structure-based virtual screening for drug discovery: principles, applications and recent advances.* Curr Top Med Chem, 2014. **14**(16): p. 1923-38.
4. Gathiaka, S., et al., *D3R grand challenge 2015: Evaluation of protein-ligand pose and affinity predictions.* J Comput Aided Mol Des, 2016. **30**(9): p. 651-668.
5. Mey, A.S.J.S., et al., *Blinded predictions of binding modes and energies of HSP90-α ligands for the 2015 D3R grand challenge.* Bioorganic & Medicinal Chemistry, 2016. **24**(20): p. 4890-4899.
6. Misini Ignjatovic, M., et al., *Binding-affinity predictions of HSP90 in the D3R Grand Challenge 2015 with docking, MM/GBSA, QM/MM, and free-energy simulations.* J Comput Aided Mol Des, 2016. **30**(9): p. 707-730.
7. Damm, K.L. and H.A. Carlson, *Exploring Experimental Sources of Multiple Protein Conformations in Structure-Based Drug Design.* Journal of the American Chemical Society, 2007. **129**(26): p. 8225-8235.
8. Knegtel, R.M., I.D. Kuntz, and C.M. Oshiro, *Molecular docking to ensembles of protein structures.* J Mol Biol, 1997. **266**(2): p. 424-40.
9. Totrov, M. and R. Abagyan, *Flexible ligand docking to multiple receptor conformations: a practical alternative.* Curr Opin Struct Biol, 2008. **18**(2): p. 178-84.
10. Paul, S.M., et al., *How to improve R&D productivity: the pharmaceutical industry's grand challenge.* Nat Rev Drug Discov, 2010. **9**(3): p. 203-214.
11. Wang, L., et al., *Accurate and reliable prediction of relative ligand binding potency in prospective drug discovery by way of a modern free-energy calculation protocol and force field.* J Am Chem Soc, 2015. **137**(7): p. 2695-703.
12. Christ, C.D. *Binding affinity prediction from molecular simulations: A new standard method in structure-based drug design?* 2016; Available from: https://f1000research.com/slides/5-1761
13. Christ, C.D. and T. Fox, *Accuracy assessment and automation of free energy calculations for drug design.* J Chem Inf Model, 2014. **54**(1): p. 108-20.
14. Lovering, F., et al., *Imidazotriazines: Spleen Tyrosine Kinase (Syk) Inhibitors Identified by Free-Energy Perturbation (FEP).* ChemMedChem, 2016. **11**(2): p. 217-33.
15. van Vlijmen, H., R.L. Desjarlais, and T. Mirzadegan, *Computational chemistry at Janssen.* J Comput Aided Mol Des, 2017. **31**(3): p. 267-273.
16. Akwabi-Ameyaw, A., et al., *FXR agonist activity of conformationally constrained analogs of GW 4064.* Bioorg Med Chem Lett, 2009. **19**(16): p. 4733-9.
17. Akwabi-Ameyaw, A., et al., *Conformationally constrained farnesoid X receptor (FXR) agonists: alternative replacements of the stilbene.* Bioorg Med Chem Lett, 2011. **21**(20): p. 6154-60.
18. Bass, J.Y., et al., *Substituted isoxazole analogs of farnesoid X receptor (FXR) agonist GW4064.* Bioorg Med Chem Lett, 2009. **19**(11): p. 2969-73.
19. Downes, M., et al., *A chemical, genetic, and structural analysis of the nuclear bile acid receptor FXR.* Mol Cell, 2003. **11**(4): p. 1079-92.
20. Feng, S., et al., *Identification of an N-oxide pyridine GW4064 analog as a potent FXR agonist.* Bioorg Med Chem Lett, 2009. **19**(9): p. 2595-8.

21. Flatt, B., et al., *Discovery of XL335 (WAY-362450), a highly potent, selective, and orally active agonist of the farnesoid X receptor (FXR).* J Med Chem, 2009. **52**(4): p. 904-7.
22. Jin, L., et al., *The antiparasitic drug ivermectin is a novel FXR ligand that regulates metabolism.* Nat Commun, 2013. **4**: p. 1937.
23. Lundquist, J.T., et al., *Improvement of physiochemical properties of the tetrahydroazepinoindole series of farnesoid X receptor (FXR) agonists: beneficial modulation of lipids in primates.* J Med Chem, 2010. **53**(4): p. 1774-87.
24. Mi, L.Z., et al., *Structural basis for bile acid binding and activation of the nuclear receptor FXR.* Mol Cell, 2003. **11**(4): p. 1093-100.
25. Richter, H.G., et al., *Optimization of a novel class of benzimidazole-based farnesoid X receptor (FXR) agonists to improve physicochemical and ADME properties.* Bioorg Med Chem Lett, 2011. **21**(4): p. 1134-40.
26. Richter, H.G., et al., *Discovery of novel and orally active FXR agonists for the potential treatment of dyslipidemia & diabetes.* Bioorg Med Chem Lett, 2011. **21**(1): p. 191-4.
27. Soisson, S.M., et al., *Identification of a potent synthetic FXR agonist with an unexpected mode of binding and activation.* Proc Natl Acad Sci U S A, 2008. **105**(14): p. 5337-42.
28. Xu, X., et al., *Structural Basis for Small Molecule NDB (N-Benzyl-N-(3-(tert-butyl)-4-hydroxyphenyl)-2,6-dichloro-4-(dimethylamino) Benzamide) as a Selective Antagonist of Farnesoid X Receptor alpha (FXRalpha) in Stabilizing the Homodimerization of the Receptor.* J Biol Chem, 2015. **290**(32): p. 19888-99.
29. Dang, L.X., K.M. Merz, and P.A. Kollman, *Free energy calculations on protein stability: Thr-157 .fwdarw. Val-157 mutation of T4 lysozyme.* Journal of the American Chemical Society, 1989. **111**(22): p. 8505-8508.
30. Jorgensen, W.L., *Free energy calculations: a breakthrough for modeling organic chemistry in solution.* Accounts of Chemical Research, 1989. **22**(5): p. 184-189.
31. Jorgensen, W.L., *Efficient drug lead discovery and optimization.* Acc Chem Res, 2009. **42**(6): p. 724-33.
32. Jorgensen, W.L. and C. Ravimohan, *Monte Carlo simulation of differences in free energies of hydration.* The Journal of Chemical Physics, 1985. **83**(6): p. 3050-3054.
33. Jorgensen, W.L. and L.L. Thomas, *Perspective on Free-Energy Perturbation Calculations for Chemical Equilibria.* J Chem Theory Comput, 2008. **4**(6): p. 869-876.
34. Kollman, P., *Free energy calculations: Applications to chemical and biochemical phenomena.* Chemical Reviews, 1993. **93**(7): p. 2395-2417.
35. Kollman, P.A. and K.M. Merz, *Computer modeling of the interactions of complex molecules.* Accounts of Chemical Research, 1990. **23**(8): p. 246-252.
36. Merz, K.M. and P.A. Kollman, *Free energy perturbation simulations of the inhibition of thermolysin: prediction of the free energy of binding of a new inhibitor.* Journal of the American Chemical Society, 1989. **111**(15): p. 5649-5658.
37. Tembre, B.L. and J.A. Mc Cammon, *Ligand-receptor interactions.* Computers & Chemistry, 1984. **8**(4): p. 281-283.
38. *Small-Molecule Drug Discovery Suite 2016-2, Schrödinger, LLC, New York, NY, 2016*.
39. *Schrödinger Release 2016-2: Canvas, Schrödinger, LLC, New York, NY, 2016*.
40. *Schrödinger Release 2016-2: LigPrep, Schrödinger, LLC, New York, NY, 2016*.
41. *Schrödinger Release 2016-2: Schrödinger Suite 2016-2 Protein Preparation Wizard; Epik, Schrödinger, LLC, New York, NY, 2016; Impact, Schrödinger, LLC, New York, NY, 2016; Prime, Schrödinger, LLC, New York, NY, 2016*.
42. Sastry, G.M., et al., *Protein and ligand preparation: parameters, protocols, and influence on virtual screening enrichments.* J Comput Aided Mol Des, 2013. **27**(3): p. 221-34.
43. *Schrödinger Release 2016-2: WaterMap, Schrödinger, LLC, New York, NY, 2016*.

44. Abel, R., et al., *Role of the active-site solvent in the thermodynamics of factor Xa ligand binding.* J Am Chem Soc, 2008. **130**(9): p. 2817-31.
45. Young, T., et al., *Motifs for molecular recognition exploiting hydrophobic enclosure in protein-ligand binding.* Proc Natl Acad Sci U S A, 2007. **104**(3): p. 808-13.
46. *Schrödinger Release 2016-2: Glide, Schrödinger, LLC, New York, NY, 2016*.
47. Friesner, R.A., et al., *Glide: a new approach for rapid, accurate docking and scoring. 1. Method and assessment of docking accuracy.* J Med Chem, 2004. **47**(7): p. 1739-49.
48. Halgren, T.A., et al., *Glide: a new approach for rapid, accurate docking and scoring. 2. Enrichment factors in database screening.* J Med Chem, 2004. **47**(7): p. 1750-9.
49. Friesner, R.A., et al., *Extra precision glide: docking and scoring incorporating a model of hydrophobic enclosure for protein-ligand complexes.* J Med Chem, 2006. **49**(21): p. 6177-96.
50. *Schrödinger Release 2016-2: Phase, Schrödinger, LLC, New York, NY, 2016*.
51. Sastry, G.M., S.L. Dixon, and W. Sherman, *Rapid shape-based ligand alignment and virtual screening method based on atom/feature-pair similarities and volume overlap scoring.* J Chem Inf Model, 2011. **51**(10): p. 2455-66.
52. Deng, Z., C. Chuaqui, and J. Singh, *Structural interaction fingerprint (SIFt): a novel method for analyzing three-dimensional protein-ligand binding interactions.* J Med Chem, 2004. **47**(2): p. 337-44.
53. Singh, J., et al., *Structural interaction fingerprints: a new approach to organizing, mining, analyzing, and designing protein-small molecule complexes.* Chem Biol Drug Des, 2006. **67**(1): p. 5-12.
54. Dixon, S.L., et al., *PHASE: a new engine for pharmacophore perception, 3D QSAR model development, and 3D database screening: 1. Methodology and preliminary results.* J Comput Aided Mol Des, 2006. **20**(10-11): p. 647-71.
55. *Schrödinger Release 2016-2: Jaguar, Schrödinger, LLC, New York, NY, 2016*.
56. Bochevarov, A.D., et al., *Jaguar: A high-performance quantum chemistry software program with strengths in life and materials sciences.* International Journal of Quantum Chemistry, 2013. **113**(18): p. 2110-2142.
57. *Schrödinger Release 2016-2: Schrödinger Suite 2016-2 Induced Fit Docking protocol; Glide, Schrödinger, LLC, New York, NY, 2016; Prime, Schrödinger, LLC, New York, NY, 2016*.
58. Farid, R., et al., *New insights about HERG blockade obtained from protein modeling, potential energy mapping, and docking studies.* Bioorganic & Medicinal Chemistry, 2006. **14**(9): p. 3160-3173.
59. Sherman, W., H.S. Beard, and R. Farid, *Use of an Induced Fit Receptor Structure in Virtual Screening.* Chemical Biology & Drug Design, 2006. **67**(1): p. 83-84.
60. Sherman, W., et al., *Novel procedure for modeling ligand/receptor induced fit effects.* J Med Chem, 2006. **49**(2): p. 534-53.
61. Clark, A.J., et al., *Prediction of Protein-Ligand Binding Poses via a Combination of Induced Fit Docking and Metadynamics Simulations.* J Chem Theory Comput, 2016. **12**(6): p. 2990-8.
62. Sastry, M., et al., *Large-scale systematic analysis of 2D fingerprint methods and parameters to improve virtual screening enrichments.* J Chem Inf Model, 2010. **50**(5): p. 771-84.
63. Zhou, R., P. Das, and A.K. Royyuru, *Single mutation induced H3N2 hemagglutinin antibody neutralization: a free energy perturbation study.* J Phys Chem B, 2008. **112**(49): p. 15813-20.
64. Kastenholz, M.A. and P.H. Hunenberger, *Computation of methodology-independent ionic solvation free energies from molecular simulations. II. The hydration free energy of the sodium cation.* J Chem Phys, 2006. **124**(22): p. 224501.
65. Kastenholz, M.A. and P.H. Hunenberger, *Computation of methodology-independent ionic solvation free energies from molecular simulations. I. The electrostatic potential in molecular liquids.* J Chem Phys, 2006. **124**(12): p. 124106.

66. Hummer, G., L.R. Pratt, and A.E. García, *Free Energy of Ionic Hydration.* The Journal of Physical Chemistry, 1996. **100**(4): p. 1206-1215.
67. Kaus, J.W., et al., *How to deal with multiple binding poses in alchemical relative protein-ligand binding free energy calculations.* J Chem Theory Comput, 2015. **11**(6): p. 2670-9.
68. Liu, S., et al., *Lead optimization mapper: automating free energy calculations for lead optimization.* J Comput Aided Mol Des, 2013. **27**(9): p. 755-70.
69. Bennett, C.H., *Efficient estimation of free energy differences from Monte Carlo data.* Journal of Computational Physics, 1976. **22**(2): p. 245-268.
70. Wang, L., et al., *Modeling Local Structural Rearrangements Using FEP/REST: Application to Relative Binding Affinity Predictions of CDK2 Inhibitors.* Journal of Chemical Theory and Computation, 2013. **9**(2): p. 1282-1293.
71. Cheng, Y. and W.H. Prusoff, *Relationship between the inhibition constant (K1) and the concentration of inhibitor which causes 50 per cent inhibition (I50) of an enzymatic reaction.* Biochem Pharmacol, 1973. **22**(23): p. 3099-108.